

**Design and Performance Characteristics of a Microfluidic Enzymatic Fuel
Cell**

BY

ROBERTO PREITE
B.S, Politecnico di Torino, Turin, Italy, 2014

THESIS

Submitted as partial fulfillment of the requirements
for the degree of Master of Science in Mechanical Engineering
in the Graduate College of the
University of Illinois at Chicago, 2016

Chicago, Illinois

Defense Committee:

Jie Xu, Chair and Advisor
Reza Shahbazian-Yassar
Pietro Asinari, Politecnico di Torino

ACKNOWLEDGMENTS

Although my name is the only one appearing in the front cover of this work, I owe my gratitude to many people.

I gladly would like to express my deepest gratitude to my advisor, Dr. Jie Xu: he was always willing to answer my questions, providing me the means to find the right direction towards the completion of this work.

My co-advisor, Dr. Pietro Asinari (Polytechnic of Turin, Turin, Italy): I am grateful to him for his suggestions and his guidance from overseas.

I am grateful to the members of Dr. Shelley Minter Research Group (University of Utah, Salt Lake City) with whom I have interacted during the course of my thesis. In particular I am thankful to Dr. Shelley Minter, Dr. David Hickey and Dr. Ross D. Milton for their patience while guiding me into the enzymatic fuel cell world. I am thankful for their kindness in providing some of the used materials for my experiment.

I am also thankful to Alireza Ahmadian Yazdi from Dr. Xu's Laboratory, for his time spent with and for me while reading my experiment reports, commenting on my ideas and helping me to broaden my views.

A big and sincere 'thank you' is for my friends Cesare, Gabriele, Marco, Leonardo, Angela, Matteo, Giuseppe, Massimo, Francesca and Camilla: despite we were scattered all over the world, you were always close to me, in the same way as we first met. Many thanks also to Andrea D.V., Andrea P., Benedetto, Marc, Lorenzo, Vittorio and all the friends that were part

ACKNOWLEDGMENTS (continued)

of this incredible adventure here in Chicago and in the U.S., sharing happy and good moments as well as the burden of the bad ones.

Most importantly, my greatest and heart-felt gratitude is for my family. Without the love, the ceaseless encouragement, the endless patience of my parents Concetta and Salvatore and my sister Francesca, literally none of this work would have been possible.

Thank you!

RP

TABLE OF CONTENTS

<u>CHAPTER</u>	<u>PAGE</u>
1 INTRODUCTION	1
1.1 Fuel Cell Basics	3
1.2 PEM Fuel Cell (PEMFC)	5
1.3 Solid Oxide Fuel Cell (SOFC)	8
1.4 Molten Carbonate Fuel Cell (MCFC)	11
1.5 Phosphoric Acid Fuel Cell (PAFC)	15
1.6 Alkaline Fuel Cell (AFC)	18
1.7 Enzymatic Fuel Cell (EFC)	21
1.8 Techniques	25
1.8.1 Fundamentals	25
1.8.2 Cyclic Voltammetry	30
1.8.3 Linear Sweep Voltammetry	36
1.8.4 Open Circuit Measurements	39
1.8.5 Polarization and Power Curves	39
2 EXPERIMENTAL SETUP	42
2.1 Anode	43
2.1.1 Glucose Oxidase	43
2.1.2 Hexylferrocenyl-LPEI (Fc-C ₆ -LPEI)	46
2.1.3 Ethylene Glycol Diglycidyl Ether (EGDGE)	51
2.1.4 Anode Coating	52
2.2 Cathode	53
2.2.1 Bilirubin Oxidase and Laccase	53
2.2.2 TBAB-Nafion	55
2.2.3 Multi Walled Carbon Nanotubes	58
2.2.4 Cathode Coating	60
2.3 Design	60
3 RESULTS AND DISCUSSION	63
3.1 Anode	63
3.2 Cathode	67
3.3 Polarization and Power Curves	70
3.4 Life and Stability	73
4 CONCLUSION	76
APPENDICES	79

TABLE OF CONTENTS (continued)

<u>CHAPTER</u>	<u>PAGE</u>
Appendix A	80
CITED LITERATURE	94
VITA	103

LIST OF TABLES

<u>TABLE</u>		<u>PAGE</u>
I	PEMFC MATERIALS	7
II	SOFC MATERIALS	10
III	MCFC MATERIALS	13
IV	PAFC MATERIALS	16
V	AFC MATERIALS	20
VI	COMPARISON BETWEEN MFC AND EFC	23
VII	DET COMPARISON.	24
VIII	BOD REACTION	55

LIST OF FIGURES

FIGURE		PAGE
1	World energy consumption from 1965 to 2014.	2
2	Fuel cells classification and schemes.	5
3	Illustration of a proton exchange membrane fuel cell.	6
4	Scheme of a solid oxide fuel cell.	9
5	Scheme of a molten carbonate fuel cell.	12
6	Scheme of an alkaline fuel cell.	19
7	Schemes of a traditional fuel cell and a biofuel cell.	22
8	Different cofactors and redox processes.	26
9	The three modes of mass transport.	30
10	Cyclic voltammetry basics.	31
11	Examples of multi-electron reversible processes.	34
12	LSV of an unstirred solution	37
13	LSV of an irreversible steady state wave	38
14	Examples of (a) polarization anf (b) power curves.	40
15	Glucose oxidase representation.	44
16	Flavin adenine dinucleotide (FAD) constitution.	45
17	Influence of pH on Fc- C_6 -LPEI.	48
18	Glucose concentration effects on redox polymers.	49
19	^1H NMR spectrum of hexylferrocenyl-LPEI.	50
20	EGDGE structural formula.	51
21	Enzymatic redox gel drop casted on the anode.	53
22	Laccase representation.	55
23	Nafion structural formula.	56
24	First steps of preparing TBAB-Nafion.	57
25	MWCNTs representation.	58
26	Comparison between OH-MWCNTs and Ac-MWCNTs.	59
27	Some of the used techniques and equipment.	61
28	Photo of the final microfluidic EFC.	62
29	CVs of the anodic coating.	64
30	CVs of a lighter anodic coating.	66
31	Comparison of BOd and laccase based cathodes.	67
32	Investigation on a MET laccase cathode.	68
33	SEM micrography and details of a toray based cathode.	70
34	Power curves comparison of BOd and laccase based EFC	71
35	Comparison of BOd and laccase based cathodes.	72
36	Life and stability of the microfluidic EFC.	74
37	Permission for Figure 2.	81
38	Permission for Figure 3.	82

LIST OF FIGURES (continued)

<u>FIGURE</u>		<u>PAGE</u>
39	Permission for Figure 4.	83
40	Permission for Figure 5.	84
41	Permission for Figure 6	85
42	Permission for Figure 8.	86
43	Permission for Table VII.	87
44	Permission for Figure 9, Figure 12 and Figure 13.	88
45	Permission for Figure 11.	89
46	Permission for Figure 17 and Figure 18.	90
47	Permission for Figure 22.	91
48	Permission for Figure 26.	92
49	Permission for Figure 27(a).	93

LIST OF ABBREVIATIONS

AFC	Alkaline Fuel Cell
BFC	Biological Fuel Cell
BOd	Bilirubin Oxidase
CHP	Combined Heat and Power
CV	Cyclic Voltammetry
DET	Direct Electron Transfer
EFC	Enzymatic Fuel Cell
EGDGE	Ethylene Glycol Diglycidyl Ether
FAD	Flavin Adenine Dinucleotide
GDL	Gas Diffusion Layer
GOx	Glucose Oxidase
LSV	Linear Sweep Voltammetry
MCFC	Molten Carbonate Fuel Cell
MCO	Multicopper Oxidase
MFC	Microbial Fuel Cell
MEA	Membrane Electrode Assembly
MET	Mediated Electron Transfer

LIST OF ABBREVIATIONS (continued)

MWCNTs	Multi Walled Carbon Nanotubes
OCP	Open Circuit Potential
OCV	Open Circuit Voltage
ORR	Oxygen Reduction Reaction
PAFC	Phosphoric Acid Fuel Cell
PBS	Phosphate Buffered Saline
PEM	Protonic Exchange Membrane or Polymer Electrolyte Membrane
SCE	Saturated Calomel Electrode
SOFC	Solid Oxide Fuel Cell
SWNHs	Single Wall Carbon Nanohorns
TBAB	Tetrabutylammonium Bromide
UIC	University of Illinois at Chicago

SUMMARY

The aim of this work is to design, build and test a microfluidic enzymatic fuel cell in order to convert the chemical energy of biofuels into electrical energy by catalyzing reactions with enzymes. Enzymatic fuel cells (EFCs) are an interesting and new research field which is very promising for micro-powering electronics. However, nowadays this technology has many challenging issues that must be solved before the possibilities of real commercial applications can be unlocked: limits related to biocatalysis and employed materials need to be overcome if EFCs are wanted to expand from the narrow range of micro power generation possibilities as they are in nowadays. For the sake of thoroughly understanding and characterizing the performances, limits and challenges of an enzymatic fuel cell, the main approach was to divide the work into two stages. First, purely electrochemical testing was performed to study the performances of the electrodes. Second, these electrodes were assembled in a microfluidic EFC and the device performance was characterized. The first stage aimed at observing the effects of enzyme immobilization, of the employed fuel/oxidant and the influence of its pH on the electrodes, as well as considering different materials or various coatings and explain the changes in the related properties; the second step was necessary for demonstrating the easiness and feasibility of a microfluidic system fabricated with novel advanced manufacturing techniques as a 3D-printing for realizing EFC devices for possible practical applications. Moreover, this latter was necessary to further study the enzyme stability, durability and the effect of fuel transport on the obtained electric power for realizing EFC devices for possible practical applications.

CHAPTER 1

INTRODUCTION

Since the beginning of the last century the world has witnessed a huge growth in energy demand, until the time of comprehension of a non-equilibrium energy outline came. Despite the past economical crisis and the still recent struggles of the world to leave it behind, as portrayed by data provided from energy agencies, energy consumption continues to increase as a product of an expanding globalization. Natural energy resources are abundant on Earth, but energy requirement from industrial societies has become impressively high. World energy supply is dominated by fossil fuel consumption (Figure 1[1]), such as coal, gas and crude oil. It makes our society question itself about when those resources are likely to be depleted. This, as the question ‘when will the world decrease its consumption of non renewable energy’, is an undoubtedly fundamental inquiry that needs a fast answer. The path chosen by our society will force it to face several scenarios, ranging from the most dangerous one to a relatively stable, similar to the actual situation. It means that the future is severely affected from how many and how expeditiously new energies will be used. In other words, our society needs a turning point, an event as important as the first industrial revolution, in order to strongly turn towards an eco-compatible, de-carbonizing and sustainable usage of various energetic sources to demolish risks of violent climate changes. Among the main contemporary issues, special importance has to be paid to the lack and difficulties of implementing successful long-term energy policies. The effectiveness of every global meeting and their related proclamations can be evaluated with

scientific data after some years; nevertheless, it becomes suddenly clear how the continuous struggle and development of new and less ambitious agreements (e.g. Copenhagen Accord, which was less ambitious than the previously made Kyoto Protocol) is an evident signal of the wasted time by this society before of an eventual 100% commitment.

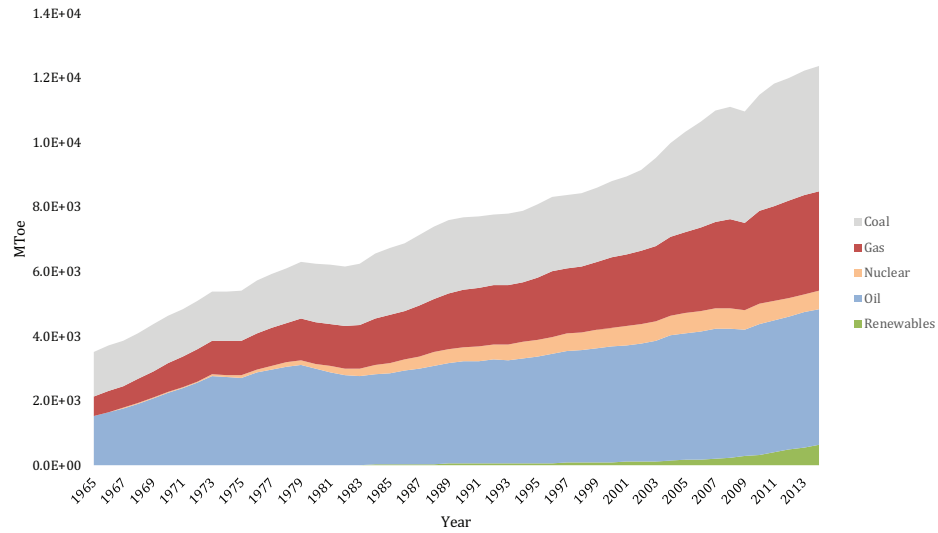


Figure 1: World energy consumption from 1965 to 2014. Data provided by BP.

However, a massive international research effort started to understand, study and try to foretell climate changing and its consequences. Starting from a Special Report on Emissions Scenarios [2], a lot has been planned and analyzed in order to better predict those six groups of possible scenarios, especially to understand how to drift away from the worst case one. The

plans, as easily imaginable due to the vast complexity of the problem, comprehended a great range of complementary options as energy saving applied to buildings, or also researching for a technology to replace fossil fuel. Among the alternatives to fossil fuel there are all those kind of biological migration options like biomass [3], which was considered by studies whose conclusions suggested the possibility to eliminate every fossil fuel use by 2100 with the aid of biofuels; the latter are assumed to be entirely produced from plants, without any usage of microbial organisms [4]. As foreseen, nowadays differentiation is playing an important role among energy researchers, especially in focusing efforts for powering micro electronics. This field is particularly demanding since it requires reliable, light, small and durable power sources. This explains how biological fuel cells (BFCs) became a principal research field involving various sectors as biology, chemistry and engineering. In general, those types of fuel cells are desirable due to their ability of generating electricity from mere renewable (bio)fuels. Other advantages are their scalability [5], which is promising for powering implantable medical devices, and the fact they operate at room temperature.

1.1 Fuel Cell Basics

In general, a fuel cell is an electrochemical device able to produce electricity starting from sources, traditionally hydrogen and oxygen. Since there is no combustion occurring, limitations from Carnot cycle do not apply to fuel cells. Despite its similarities with a battery since they both produce electrical energy through an electrochemical process, a fuel cell consumes external substances thus it can operate uninterruptedly as far as fuel and oxidant are supplied to the system. The maximum work that a fuel cell can provide is equal to the variation of free energy

$[G]$ related to the fuel combustion as shown in Equation 1.1:

$$W_{el} = -\Delta G \quad (1.1)$$

A fuel cell has electrodes made by porous materials and they are separated by an electrolyte. Each electrode acts as a catalytic site for reactions basically producing water and current throughout an external electric circuit. The electrolyte is crucial since it moves ions produced by one reaction to the other electrode where those ions are being consumed. In this way, the internal electric circuit is closed. Normally the electrochemical transformation presents heat generation, which should be extracted to keep the working temperature of the cell constant. The first type of fuel cells that was discovered was based on hydrogen, but all the category works in the same way: fuel (hydrogen) is supplied to anode, where a catalytic oxidation occurs. Among the products of this reaction there are electrons which are conducted by an external electrical circuit, therefore electricity is produced. This circuit leads the electrons to the cathodic region, where they react with an oxidant (oxygen) and protons that were permeating through an electrolyte membrane, hence the product of this reaction is formed (generally water) [6].

(Equation 1.4) is the overall reaction formula obtained by summing the previous half-reactions.



Fuel cell performances are deeply affected by thermodynamic factors [7] (e.g. the cell operating temperature, pressure and chemical concentration of species involved) and by electrochemical kinetics of the reactions occurring at the electrodes. In this chapter several types of fuel cells (Figure 2) will be presented with the aim of providing a concise but comprehensive knowledge about the categories kin to the EFC.

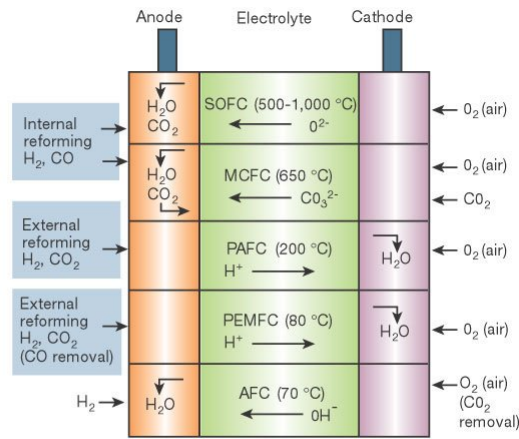


Figure 2: Fuel cells classification and schemes. Reproduced from [7]. Copyright Nature.

1.2 PEM Fuel Cell (PEMFC)

To avoid short-circuit of the cell, a membrane called Protonic Exchange Membrane (PEM) is used (Figure 3 [8; 9]). It owes its name to the usage of a special polymer electrolyte membrane:

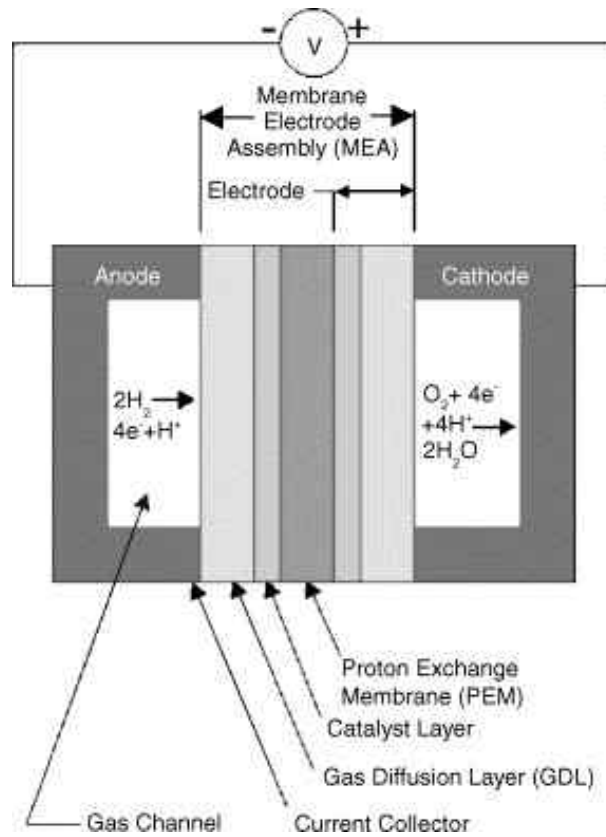


Figure 3: Illustration of a proton exchange membrane fuel cell. Reproduced from [8]. Copyright Elsevier.

this semipermeable membrane (porous to ions H^+ , waterproof for the used gases and to the electrons) must resist to the reducing cathodic environment and to the oxidant anodic one. Usually the most employed type is a Nafion based membrane that is able to conduce only up to 80-90 °C: above this temperature it does not work due to drying. Electrodes are made of porous carbon coated with catalysts such as platinum or its alloys (see Table I). With respect to other fuel cells types, PEMFCs present higher power density in stacking (more than 1.3 kW/kg),

TABLE I: PEMFC MATERIALS

Anode	Gas Diffusion Layer (GDL) electrodes composed of a diffusive layer (carbon and PTFE) and a catalytic layer on carbon paper or carbon cloth Platinum or Pt-based alloy as a catalyst. About $0.2 - 0.4 \text{ mg/cm}^2$
Cathode	
Electrolyte	Sulfonated membrane (Nafion type) thick up to $200 \text{ }\mu\text{m}$

almost no corrosion since the electrolyte is employed in form of a polymer. In addition, they are relatively simple to manufacture and they have a quick startup (about one minute). However, due to their low operative temperatures, a PEMFC suffers if CO content in the fuel is greater than 10 ppm since carbon monoxide leads to catalyst poisoning at the anode [10]. In order to mitigate the latter disadvantages, research is focused on developing high temperature resistant membranes.

PEMFCs are made up of an anode in which hydrogen oxidation occurs (Equation 1.2), a cathode where there is oxygen reduction (Equation 1.3) and a polymeric electrolyte. These three parts are assembled together in a structure commonly referred as MEA (Membrane Electrode Assembly) [11]. Normally, PEMFCs use GDL electrodes which have a diffusive layer composed by a mixture of carbon and PTFE: this layer aims to diffuse reagent gases with a catalytic region characterized by a mixture of carbon/platinum with a polymer. The vast majority of this type of fuel cells employ perfluorinated membranes like Nafion (produced by DuPont, but other perfluorinated polymers exist), since they have high chemical and long term stability both in reducing and oxidizing environments. Typical value of their resistance is $0.05 \text{ }\Omega/\text{cm}^2$. It must be reminded that this type of membrane should always work in wet conditions in order

to enhance protons conductivity (around 0.1 S/cm). Despite this, an excessive wetting must be avoided since it would not further boost the protons conductivity but it will enlarge the electrode, causing therefore an increase in gas diffusion resistance. It should be noticed that less thickness (typically is under $200\text{ }\mu\text{m}$) means an easier wetting but also greater permeability and less mechanical strength. Hence it can be easily explained the recent development of reinforced membrane $30\text{ }\mu\text{m}$ thick or less. They are constituted by a matrix of PTFE soaked with a Nafion-like liquid electrolyte. Despite PTFE enhances both mechanical strength and specific resistance, thanks to the lower thickness the increase of the resistance does not affect the cell performances.

Actual research aims to develop membranes able to withstand operative conditions for higher temperature [13]: this is due to making easier an integration of PEMFCs into automotive systems or either for coupling them with fuel treating systems. The existence of membranes capable of working at temperature higher than $100\text{ }^{\circ}\text{C}$ will open the possibility to build cells able to accept CO content highly superior to 10 ppm.

1.3 Solid Oxide Fuel Cell (SOFC)

A SOFC is characterized by the usage of a solid oxide or a ceramic as electrolyte, i.e. gadolinium doped ceria, scandia stabilized zirconia and yttria-stabilized zirconia. This typology of fuel cells operate at temperature higher than PEMFCs: about $800\text{-}1000\text{ }^{\circ}\text{C}$ are necessary to guarantee a sufficient conductivity to the electrolyte. There are different configurations available for SOFCs, depending on the cell shape, dimensions and thickness required to the components, geometry of the channels for reactant gases. State of the art geometrical config-

urations are tubular type and planar one. Although different setups may exist, the choice of materials is independent from the chosen design. As reported in Table II, usually the anode is made of a cermet of nickel oxide and zirconia (despite attempts of building nickel-free anodes have been reported [14]), while the cathode is based on strontium-doped lanthanum manganite (at the beginning noble metals were used; nowadays electronically conducting oxides are employed to cut costs [15]). Since all components are solid, a SOFC lacks of issues typical of fuel cells with liquid electrolyte, such as resistance to corrosion and evaporation. The high working temperature enables the dismissal of particular requirements for the fuel like converting it before supplying the latter to the cell, since this phenomenon occurs inside the stack. Thus, the employed gas can be directly injected into the assembly, resulting in remarkable simplifications for the system. Figure 4 [16] hints that the following reactions occur:

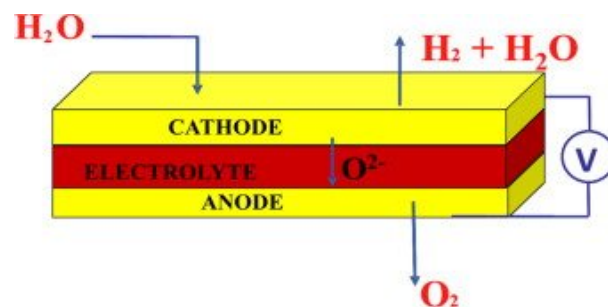


Figure 4: Scheme of a solid oxide fuel cell. Reproduced from [16]. Copyright Elsevier.

TABLE II: SOFC MATERIALS

Anode	Cermet Ni-ZrO ₂ ; thickness \approx 150 μ m, porosity 20-40%. Fabricated by slurry-coat, EVD or plasma spray
Cathode	La(Sr)MnO ₃ ; thickness \approx 2mm,porosity 30-40%. Fabricated by extrusion or sintering
Electrolyte	ZrO ₂ (Y ₂ O ₃); thickness \approx 40 μ m. Fabricated by EVD



A SOFC has various resemblances with a molten carbonate fuel cell due to the fact that there is a migration of O^{2-} ions from the cathode to the anode, where water is then formed, beneath the ceramic electrolyte: once the threshold of 800 °C is overcome, the electrolyte made of zirconia allows O^{2-} ions conduction.

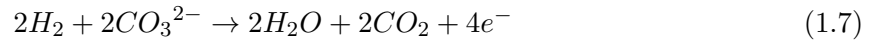
Nowadays further efforts [17] have been made to reduce the high working temperature below 600 °C to cut down costs and open new applications. Nano-engineering has been witnessing an enormous interest to enhance advanced active electrodes surfaces for SOFCs [18]. Because of a working temperature around 1000 °C, the heat released by SOFCs can be further used in combined cycle [19], especially with gas turbines. For these combined cycles, expected values of electrical efficiency are higher than 60%, with peaks of 70% reached by the major producer of SOFCs (Siemens). High efficiency systems integrating SOFC technology can be realized within the power range from 250 kW beyond 25 MW, and they represent the best solution

in terms of highest efficiency about distributed electricity generation. Among the various fuel cells technologies, considering both working temperature and the employed material, a SOFC is the only one with a potential to be competitive in the market for small size (residential and portable usage, inferior than 5 kW) and for plants of about 20 MW (for distributed power generation). SOFCs can also be used as auxiliary power units for transport applications.

1.4 Molten Carbonate Fuel Cell (MCFC)

A MCFC is based on a solution of alkali metal carbonates at a temperature close to 650 °C which gives high conductivity to the electrolyte. This solution is held in a porous ceramic matrix, with electrodes made by nickel alloys: nickel-chromium at the anode, lithiated nickel oxide at the cathode. With respect to low temperature fuel cells, MCFCs have some advantages like quicker kinetics of reactions, thus there is no need of precious metals for catalysis. Furthermore, they guarantee more flexibility with regards to the fuel choice since there is the opportunity to fuel the cell directly with natural gas or light distillates without externally reforming the fuel. It is also possible to apply CHP at temperatures useful for industrial applications.

As showed in Figure 5 [20], reactions occurring in a MCFC are:



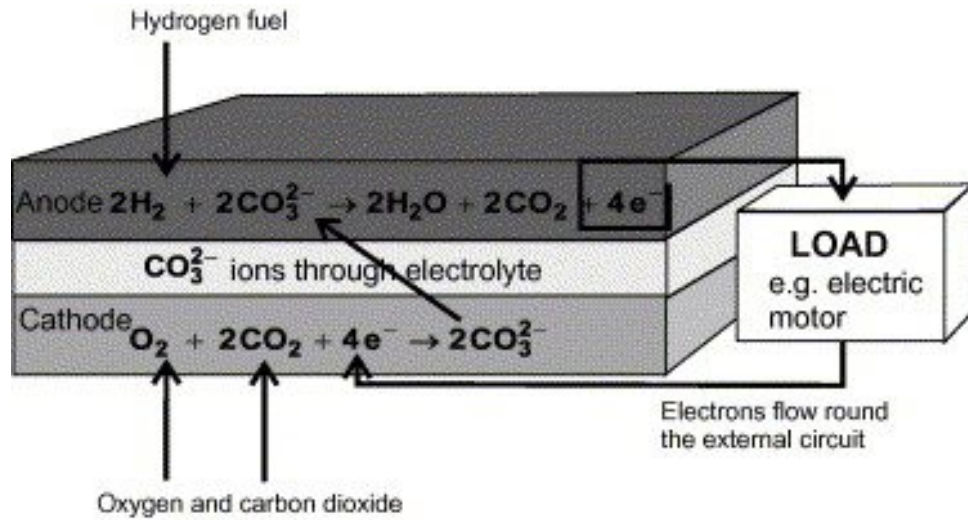


Figure 5: Scheme of a molten carbonate fuel cell. Reproduced from [20]. Copyright Elsevier.

When a hydrogen rich gas is obtained by reforming or by carbon gasification, anodic reactions involves both hydrogen and carbon oxide. If that is the case, CO reacts with the just produced water (it is the opposite of what happens in PAFCs), giving additional hydrogen as result:



Carbon dioxide flowing out the anode is recycled at the cathode. MCFCs are scarcely tolerant to sulfur compounds like H_2S or COS. Oxygen is supplied to the cathode as well, providing carbonate ions as a product of Equation 1.8. Carbonate ions flow through the electrolyte towards the anodic environment, where they are changed back into carbon dioxide (Equation 1.7).

There are different methods used to provide CO_2 at cathode:

TABLE III: MCFC MATERIALS

Anode	Nickel-chromium or Ni-Al; surface area $0.1 - 1 \text{ m}^2/g$; thickness 0.2 - 0.5 mm
Cathode	Lithiated NiO-MgO; surface area $0.5 \text{ m}^2/g$; thickness 0.5 - 1 mm
Electrolyte	$Li_2CO_3K_2CO_3$ at 6238% or $Li_2CO_3Na_2CO_3$ at 60-40%; thickness 0.5 - 1 mm

- a. from an external supply source;
- b. exploit a membrane separator to divide carbon dioxide from the gas flowing out of the anode. The extracted CO_2 is moved to the cathodic gas inlet;
- c. employ a burner to recycle it after picking it from the anode. In this way all the unused hydrogen/fuel will be converted into CO_2 and water, and the waste heat will be used for other applications.

Option *c* is the most commonly adopted choice.

As reported in Table III, actually anodes are composed of Ni-Cr or Ni-Al alloys, with porosity around 60-55% and thickness from 0.2 to 0.5 mm. A typical anode structure is obtained by casting and sintering fine powder, or by hot pressing. Chromium is a necessary metal since it decreases nickel sintering while the MCFC is running; at those high temperature, it will help to control porosity, surface area and mechanical stress under compression. All the previously factors can cause a decrease of performances. On the other hand, chromium is an element able to react with lithium inside the electrolyte; luckily, by adding a small percentage of aluminum this issue can be prevented. In addition, aluminum enhance creep resistance of the anode due to the constitution of $LiAlO_2$ inside nickel particles. Researcher's efforts have been focusing

on developing alternative materials to sharply decrease costs or to enhance sulfur tolerance in the fuel stream (in this case, anodes made by ceramic). Porosity can be controlled during the manufacturing process: it is preferred to have big pores near the fuel flow. The main issue faced is the long term life and management of the electrolyte [21].

State of the art MCFC cathodes are based on lithiated NiO-MgO. One of their main issues is that they have a considerable solubility in molten carbonates which leads to nickel ions formation [22]. By diffusion, the above-mentioned ions moves to the anode and metallic nickel precipitate in the electrolyte: this may be an important issue since it can be a sink for Ni ions (hence enhancing nickel dissolution from the cathode) or an internal short circuit could occur. Dissolution is proved to be reduced when using more basic than acidic carbonates into the electrolyte. Practical ways to control and decrease dissolution rates are to use a thick electrolyte matrix, to operate at atmospheric pressure, to use a basic carbonate and to set a low value of CO_2 partial pressure in the cathodic environment. With all these precautions, a single cell can work up to 40000 hours.

A typical electrolyte is a solution at 60-40% of $Li_2CO_3Na_2CO_3$. Until the late Eighties, the matrix was produced in a tile form by hot pressing. Today, it is produced with more conventional methods like tape casting: ceramics are added in a solvent with already dissolved plasticizers, binders and several additives for reaching the wanted viscosity. The second step of this process is the cast over a moving surface, where thickness is mechanically controlled by a blade. After that, film is dried and heated to remove all organic binders. This process is useful when the aim is to produce a large area component. Unfortunately, in a MCFC about 65-70%

of ohmic losses have to be accounted to the electrolyte; it has to be reminded that a high ohmic resistance is a strong limit for current density. However, on the other hand tape casting helps to reduce the ohmic resistance by achieving thickness values around 0.5 mm.

Although with MCFCs it is perspective possible to realize plants with efficiency levels higher than the ones coming from low temperature fuel cells (real values are around 45%, with peaks of 70% when coupling together with a turbine cycle), their high working temperature and the grand electrolyte corrosiveness are among the big structural stability issues that limit this technology. Among the other critical points there are cathode dissolution in lithium oxide, anode sintering and corrosion of the bipolar plates. Therefore, despite all the giant progresses achieved during the time, there is still plenty of work to do to overcome those problems and finally reaching the necessary aims to produce electric energy (at least 40'000 working hours for stacking and plants cost inferior than 1'500 \$/kW) [23].

1.5 Phosphoric Acid Fuel Cell (PAFC)

The structure of a Phosphoric Acid Fuel Cell (PAFC) is very similar to a PEMFC, but in this case the electrolyte is made of a concentrated solution of phosphoric acid H_3PO_4 which enables protons conduction. A PAFC works at temperature near 200 °C: its working temperature is high enough to avoid usage of extremely pure supply gases but also not so extreme to present materials related issues. Therefore it is possible to employ gases coming from hydrocarbons reforming processes without any intermediate purification step required. This type of cell is characterized by a high electrical efficiency which ranges from 37% to 42%. PAFCs are part of a technology which is especially developed in Japan and USA. Moreover they are ready to

TABLE IV: PAFC MATERIALS

Anode	Platinum and PTFE on carbon support (Vulcan XC 72) About 0.1 mg/cm^2 of Pt
Cathode	Platinum and PTFE on carbon support (Vulcan XC72) About 0.5 mg/cm^2 of Pt
Electrolyte	100% H_3PO_4 on PTFE-SiC amorphous matrix

be used for electricity generation and small-medium size CHP. PAFCs made possible to build systems and plants with different characteristics and power ranging from 50 kW up to 11 MW.

Those are the reactions occurring in a PAFC:



As in PEMFCs, water formation occurs at cathode and it is expelled with surplus air into the exhaust gas of the cathodic compartment. Only hydrogen is involved in the process. If the system is designed to work with synthesis gas it is mandatory to convert the eventual carbon monoxide CO into carbon dioxide and hydrogen. This is a fundamental step which cannot be avoided since if there is carbon oxide (maximum allowed CO percentage is 1%) into the gas supplied to the anode, there will be poisoning of the catalysts. In addition, carbon monoxide reduces the PAFC efficiency.

The employed electrolyte (H_3PO_4 , see Table IV) has particular properties: it has good electrochemical and thermal stability, plus it resists to the carbon dioxide if the latter is contained into the fuel or the oxidant. This viscous and transparent acid is used within a layer (thickness up to 0.2 mm to avoid high ohmic losses) of porous amorphous matrix made by silicon carbide particles and PTFE; those particles have a diameter of maximum 1 μm , providing good mechanical properties and avoiding crossover of gases coming from the anode and cathode (as far as the pressure difference between anode and cathode does not exceed 200 mbar). Carbon is employed with PTFE for supporting the electrode structure (see Table IV). Moreover, carbon provides enough micro-pores to enhance diffusion between gas and catalysts while maximizing the surface contact with electrodes; it raises the electrical conductivity and helps scattering the catalyst all over the electrode.

Platinum is used a catalyst and there are different parameters that can be varied in order to characterize the electrodes, like the specific surface area and the crystallite size: one can achieve a high activity of catalyst by coupling small crystallites with high surface area. Apparently this can be misleading: how is it possible that now platinum usage was reduced to 0.5 mg/cm^2 ? This was made possible thanks to crystallites as small as 2 nm and surface areas as high as 100 m^2g^{-1} . PTFE is employed as a "glue" to tie carbon black particles together in a resulting porous layer [26] (actual values are about 60% for a wet proof layer with micro-pores of 3.4 nm and macro-pores up to 50 μm) which lies on a substrate composed by carbon paper. The latter also aims to collect the current and to provide structural support for the electrodes. The "final" composite structure (carbon black/PTFE on carbon paper) helps to stabilize the

three-phase interface which has to deal with two different environments: the one containing the electrolyte and the other on which there is the reactant. In addition to find some proper methods to correctly scatter the platinum, it is crucial to heat treat nitrogen to boost corrosion resistance of carbons in this type of fuel cells. However, electrode performances will degrade over time due to the migration of platinum particles and the electrolyte flooding which will result in the blockage of the gas throughout the structure. Temperature strongly influences the agglomeration process. Both of those phenomena cause a decrease in the active surface area, therefore also in the produced current. However, about 40'000 hours of operations can be achieved as a lifetime of electrodes. Experience suggested that the best operative conditions for PAFCs are far away to work above 0.8 V (otherwise carbon corrosion significantly occurs); in addition, it is strongly desisted to get low current densities or hot idling with an OCP.

1.6 Alkaline Fuel Cell (AFC)

As before, alkaline fuel cells (AFCs) owe their name to the employed electrolyte, which needs to be an alkaline solution like sodium hydroxide NaOH or potassium hydroxide KOH. Note that in an AFC, the two half-reactions are different since in an alkaline electrolyte there is only availability of OH^- ions which are formed by reaction occurring at the cathode between oxygen and electrons coming from the anode. Although the two half-reactions are different as depicted in Figure 6, the whole reaction is the same as in Equation 1.4. Water is formed at anode where it is removed with residual hydrogen. An alkaline fuel cell requires extremely pure supply gases, with at least 99.9 % of purity. It can not tolerate carbon compounds like carbon oxide and dioxide due to their interaction with the electrolyte.

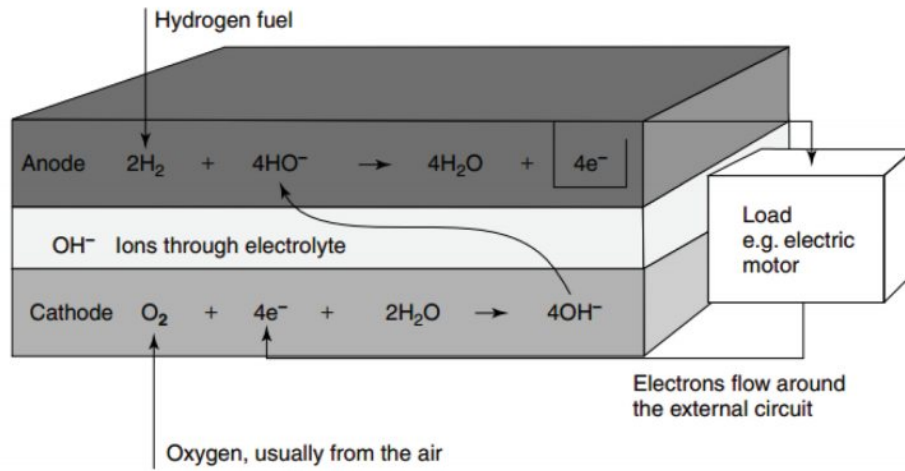


Figure 6: Scheme of an alkaline fuel cell. Reproduced from [27]. Copyright John Wiley and Sons.

AFCs operate at low temperature, typically in a range from 70°C to 120°C . Usually the employed electrolyte is an aqueous solution of potassium hydroxide KOH (see Table V) that flows through the cell or it is stored in a matrix of asbestos. Compared to other low temperature operating fuel cells, AFCs have several advantages like electrical efficiency as high as 65%, not expensive cell components and long lifetime (about 15'000 hours due to a good compatibility between cell materials). Among the principal defects there is a low tolerance towards impurities of supply gases; OH^- ions react with carbon compounds, even if there are only traces, therefore it is difficult to use synthesis gas obtained with reforming process. In addition, even air usage shows problems due to CO_2 presence superior to 300 ppm, but by using an absorbing tower the CO_2 content can be controlled. This explains why it is necessary to provide extremely pure gases or, alternatively, to utilize complicated and expensive purification systems: thus, it is not

TABLE V: AFC MATERIALS

Electrodes	Nickel, silver, noble metals like platinum/palladium
Electrolyte	30-45% KOH solution flowing through the cell or on an asbestos matrix

economically convenient to exploit AFCs for stationary electrical energy production. Despite achieving a good maturity from a technological point of view, commercial and research activities are very limited in this sector. In the past researchers focused on developing systems for military use or for powering transportation vehicles. It should be reminded that this technology has been successful employed in many NASA space missions since 1960s (keeping in mind that only pure hydrogen and oxygen are present in space vehicles).

On the other hand there were a lot of examples showing how many problems had to be solved, like safety, costs, reliability and so on. In addition, at that time there were different technologies that were considered more feasible than AFCs. Also, the recent re-discovered interest for PEMFCs contributed to AFCs decay. Nevertheless, they have several advantages over other kind of fuel cells like a lower activation cathodic over-voltage that usually is the greatest loss for a low temperature operating fuel cells. Plus, an AFC assembly is not so expensive since it employs non precious metals for electrodes and a very cheap electrolyte.

About the AFC configuration, the characterizing factor is how the electrolyte is used in the system, since KOH can flow through the cell (the most employed solution) or it is trapped in an asbestos matrix.

1.7 Enzymatic Fuel Cell (EFC)

Enzymatic fuel cells (EFCs) are a promising and rising research field that employ renewable (bio)fuels and catalysts to obtain electrical energy. Their working principle is exactly the same of a traditional fuel cell: an electrolyte divides an oxidant reducing cathode from a fuel oxidizing anode. Each electrode is built to avoid usage of expensive and non-selective catalysts like platinum. Furthermore, platinum and its alloy presents the issue of catalysts deactivation due to poisoning, that can easily explain why enzymes are used. It is true that the choice of a certain type of enzyme depends on several factors that will be explained later in this chapter. In general, an EFC works under conditions like neutral pH and room temperature, hence it is more favorable than other fuel cells. Since it uses a concentrated source of energy, it has a high efficiency in converting it into electric energy (this is a property of every bio-fuel cells): furthermore, it is possible to reduce its dimensions and weight to implant them in living organisms to harvest fuel from their surrounding environment.

In Figure 7 [28] there is a comparison between a typical PEMFC and an EFC. It is very important to notice that if an EFC uses highly selective enzymes coated on its electrodes, a membrane becomes an avoidable surplus.

As suggested by its name, the core of an enzymatic fuel cell is the chosen enzyme [33], which in turn characterizes the electron transfer mode. For instance, a redox enzyme is made of the main protein called 'apoenzyme', and one or multiple non-protein known as 'cofactors'. The latter are responsible of the electron transfer between electrode and enzyme. In Figure 8 [34] there are schematics of the most employed cofactors and their redox process. Historically, the

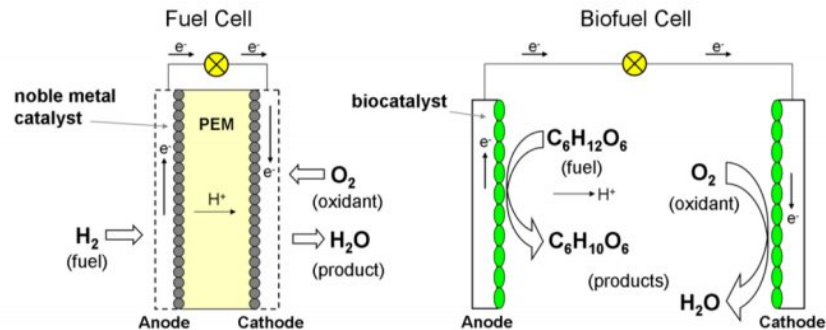


Figure 7: Schemes of a traditional fuel cell and a biofuel cell. Reprinted from [28]. Creative Commons Attribution License.

first processes that had been studied were based on mediated electron transfer (MET); as suggested by the name, a mediator is employed to enhance the thermodynamic redox potential of the process. This mediator, which can be a redox hydrogel, a crosslinker etc, literally carries electrons between the enzyme and its substrate, therefore it must possess a good electro activity to enhance anodic potential, and to decrease cathodic reductive one. On the other hand, direct electron transfer (DET) is one among the major development in EFC due to its ability at overcoming issues related to the usage of mediators (i.e. design issues, chemical ones, trade offs to avoid since a mediator enhances the driving force while increasing cell voltage losses [35]).

Since the rate of electron exchange, thus current, is an output exponentially proportional to the distance between an electron acceptor and donor, it is clear why DET is important. However, this way of electron exchange occurs only when the substrate is within 2 nm [36] from the cofactor (active site in which the redox/oxidizing reaction is happening). In Table VII [37]

TABLE VI: COMPARISON BETWEEN MFC AND EFC

Microbial Fuel Cell	VS	Enzymatic Fuel Cell
Sugars fully oxidized to CO_2 [29]	<i>Fuel</i>	Sugars partially oxidized
Long lifetime, more than four years [30]	<i>Life</i>	Brief lifetimes, around a week [31]
Low power densities due to cellular membranes [32]	<i>Power density</i>	Higher than MFCs, but still lower than conventional ones

there is a comparison in the employed materials and their related performances among several DET based EFCs. Usually the greatest cell voltage for an EFC is detected from the formal redox potentials $E^{0'}$ of the redox enzyme cofactor(s) employed for the anodic and cathodic site. There are two different approaches to build an EFC: decide to use an enzyme cascade to extract up to 24 electrons from glucose, or employ a single enzyme at the anode to obtain 2 electrons from the oxidation of glucose into gluconolactone. On one hand the first solution allows to reach greater current peaks, but on the other hand it has to take into account issues like fuel degradation, trade-offs in pH level etc that inevitably force the enzymes of the employed cascade not working in their best efficiency point [47]. Lastly, among the solutions available to overcome EFCs defects such as the brief life of the enzyme (about 2 days in buffer solutions), immobilization techniques have been developed. Although the latter can provide a drop in the cost because of smaller quantities -and with longer life- employed, coupled with great enzyme and output stability, on the other hand immobilization of enzymes often mean lower power

TABLE VII: DET COMPARISON. REPRINTED FROM [37]. COPYRIGHT ELSEVIER.

Fuel Oxidant	Anode Cathode	Solution	OCV (V)	Power ($\mu\text{m}/\text{cm}^2$)	Stability (h)	Refs.
H_2 O_2	Hd/Lc	Citrate-PB pH 8 anolyte; pH 4.2 catholyte	1.35	400	>168	Tarasevich et al. [38]
H_2 O_2	MBH/Lc	Acetate buffer pH 6, 10 mM glucose and EtOH	0.97	7	>0.25	Vincent et al. [39]
$EtOH$ H_2O_2	ADH/MP- 11	Citrate buffer pH 5, bubbling of H_2 and air	0.27	0.2	~60	Ramanavi- cius et al. [40]
<i>Fructose</i> O_2	FDH/Lc	McIlvaine buffer pH 5, 200 mM fructose and O_2 sat.	0.79	840	>12	Kamitaka et al. [41]
<i>Fructose</i> O_2	FDH/Lc	Citrate buffer pH 5, 200 mM fructose and bubbling of air	0.66	126	~87	Wu et al. [42]
<i>Glucose</i> O_2	CDH/Lc	Citrate buffer pH 4.5, 5 mM glucose	0.73	>5	~ 25	Coman et al. [43; 44]
<i>Glucose</i> O_2	CDH/BOx	PBS pH 7.4, 5 mM glucose Serum	0.62 0.58	3 4	>6 <2	Coman et al.[44]
<i>Glucose</i> O_2	GOx/Lc	PBS pH 7.4, 5 mM glucose Blood	0.23 0.12	30 5.6		Pan et al. [37]
<i>Glucose</i> O_2	GOx/Lc	PB pH 7, 50 mM glucose	0.95	1300	~ 2.76	Zebda et al. [45]
<i>Glucose</i> O_2	CDH/BOx	PBS pH 7.4, 5 mM glucose	0.66	3.2	~30	Wang et al. [46]
		Blood	0.66	2.8	~2	
		Plasma	0.63	3	~8	
		Saliva	0.63	2.1	~ 1	
<i>Glucose</i> O_2	CDH/BOx	Tears	0.57	3.5	>10	Falk et al. [37]

output with respect of EFCs using enzymes dissolved in solution. Undeniably EFCs are part of a promising and recent research field as demonstrated by the sharp increase of publications; however, future challenges regard coupling EFC with MFC or miniaturization of the latter category to improve biomimicking of the involved proteins in order to reach further superior threshold of power, electric current and/or stability [48]. A great challenge would be an actual implementation of remote/portable devices to use in ordinary life: this concept has been recently proved to be feasible for medical devices [49] or contact lenses [50].

1.8 Techniques

Since EFCs are a relatively new branch of fuel cells, the most natural step to study them was to adapt, refine and further develop already existent analytical, theoretical and experimental techniques. Because of the biology involved in this technology, every change regarding the employed catalysts or materials can be observed by a wide usage of certain graphs. The above mentioned plots come from various electro-chemical tests that will be now explained. Firstly, some fundamental electrochemical concepts are presented.

1.8.1 Fundamentals

There are two different kinds of electrochemical tests: potentiostatic and potentiometric, which both involve at least two electrodes into an electrolyte solution. The working electrode reacts to the analyzed analyte [52], while the reference electrode is kept at a constant potential as it is independent on the solution's characteristics. This system is constituting an electrochemical cell which is defined 'galvanic' if it generates electrical energy, otherwise it is "electrolytic" if it drains electrical energy. Tests defined as potentiostatic consider the analysis

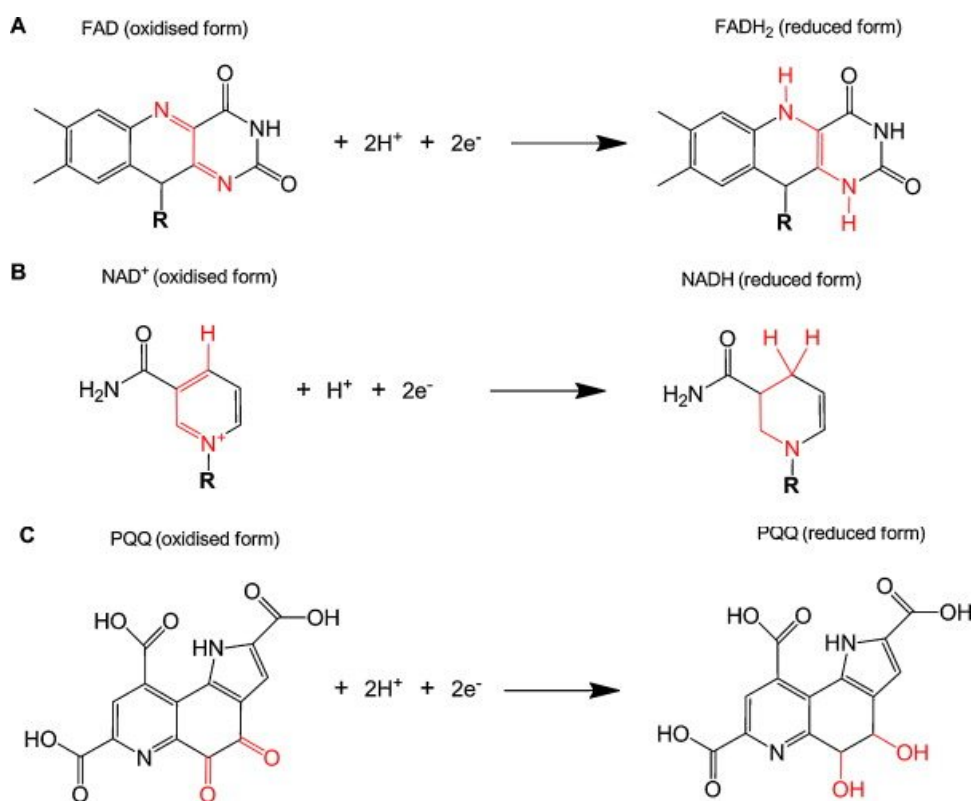


Figure 8: Different cofactors and redox processes for A) *FAD*/*FADH₂*, B) *NAD* + /*NADH* and C) *PQQ*. It is reminded that R connects adenosine diphosphate (ADP) via ribitol to the flavin (case A) or nicotinamide (case B). Reprinted from [34]. Copyright Elsevier.

of the interface between the employed solution and the selected electrode, hence they are necessary to investigate about the electron transfer in situations for which the current is different than zero. Every potentiostatic technique is useful to inquire about any electroactive - therefore directly involved in an electron transfer process - chemical species. Potentiostatic tests are useful since they are extremely selective, sensitive, they present an extended linear range, and

the used equipment is relatively portable and low cost. Furthermore, it is possible to employ different types of electrodes.



This reaction represents a reversible redox process of an analyte where R is the reduced form of the redox couple while O is the oxidized one. This is a reaction happening around a potential value such that the electron transfer become favorable from the thermodynamic point of view.

The most important rule is expressed by Nernst equation:

$$E = E^0 + \frac{2.3RT}{nF} \log \frac{C_O(0,t)}{C_R(0,t)} \quad (1.13)$$

It is reminded that E_0 is the standard potential of the redox couple, R the universal gas constant, T the temperature, n the amount of exchanged electrons, F the Faraday's constant, while C_O and C_R are respectively the concentration of the oxidized and reduced forms. From Equation 1.12 it results a current called "faraidic" since it is described by Faraday's law, hence by measuring faraidic current value it is possible to determine the rate of the redox reaction. That is why during an experiment it is important to reduce the non-faraidic current, which basically is the one produced by ion exchange into the electrolyte. Supposing that the resulting current is being measured while O is reducing, in order to have a discharge it is mandatory that the oxidized form reaches the working electrode surface to receive electrons from there. Hence, the discharge process is ruled by two different kinetic factors: the migration rate in which the chemical species arrives to the surface of the working electrode and the exchange

rate for which electrons go through the electrode into the solution. Assuming that the electron transfer is almost instantaneous: in this case, discharge is mainly due to the slowest process (the first one), hence it depends on how the oxidizing form reaches the electrode. Therefore, in this situation, there are identical conditions as in a solution under electrolysis, thus the current flowing is depending on convection, migration and diffusion phenomena like in electrolysis. What influences if a certain reaction is being driven by electron exchange or mass transport? The answer is complex, since it depends on different experimental conditions, thus the involved type of mass transport, the analyzed compound, the electrode material and so on. That may explain why for certain systems the limit may be influenced on the potential window under observation. Regarding again the above-mentioned case in which the whole reaction is only controlled by the electron transfer, this means that the current is "mass transport limited". All of these cases belong to the nernstian/reversible reactions.

Mass transport can be influenced by three modes: convection, migration and diffusion (Figure 9). Convection is the phenomenon involving a movement of the analyte and solvent, due to an aroused solution. Indeed a turbulent motion develops in this solution, which becomes laminar in the electrode proximity; on this latter, the fluid layer is practically stationary, hence it has zero velocity. In addition to mechanical agitation, convection can be caused by temperature or density gradients: they generate a flux of matter which re-establish equilibrium all around the solution. The motion of electrical charges (associated to ions due to convection) generates an electrical current inside the voltammetric cell. Migration occurs when the ions motion is driven by the attractive force of the electrical field generated by the electrode of the opposite

sign. This ion migration produces a charge motion that develops an electrical current inside the voltammetric cell. In Figure 9 the electro-active species are cations going towards a cathode which, in this case is negative since the cell is electrolytic. The half-reaction is a reduction. Lastly, there is diffusion, which is the spontaneous motion driven by concentration gradients: with diffusion, the system tries to restore homogeneity. After discharge has occurred, nearby the electrode, the concentration of the electro-active species decreases, and that generates a concentration gradient which pulls back the discharging species with a diffusion rate directly proportional to the concentration gradient. Since the concentration of the species is practically zero at the boundaries of the electrode, the diffusion generated electrical current is proportional only to the concentration of the analyte, allowing to perform quantitative analysis on this analyte.

Nernst-Planck equation (Equation 1.14) allows to compute the flux J [mol/(cm²s)] of mass transport at a certain point:

$$J(x, t) = -D \frac{\partial C(x, t)}{\partial x} - \frac{zFDC}{RT} \frac{\partial \phi(x, t)}{\partial x} + C(x, t)U(x, t) \quad (1.14)$$

New terms are D diffusion coefficient [cm²/s], $\frac{\partial C(x, t)}{\partial x}$ is the concentration gradient, z is the charge of the analyzed species, $\frac{\partial \phi(x, t)}{\partial x}$ is the potential gradient, while $U(x, t)$ is the hydrodynamic speed. Thus, Nernst-Planck equation describes a quite complex situation when the previously mentioned three modes of mass transport are occurring at the same time. Nevertheless, diffusion can be predominant by using a quiescent solution to cut down convection motion, plus employing a high concentration of the support electrolyte to decrease the migration effects.

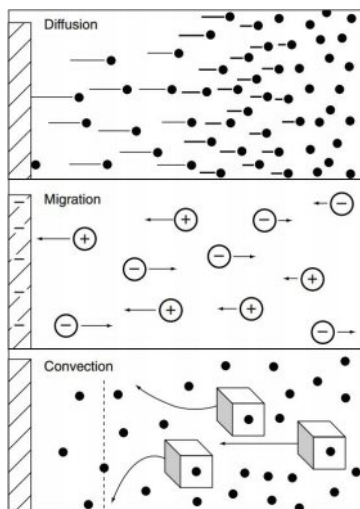


Figure 9: The three modes of mass transport. Reprinted with permission from [51]. Copyright 2016 American Chemical Society.

This leads to:

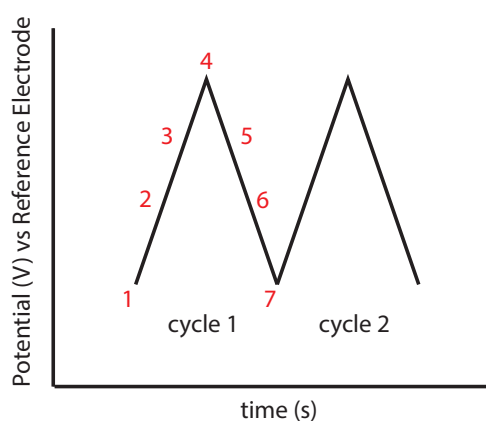
$$i(t) = nFAD \left. \frac{\partial C(x, t)}{\partial x} \right|_{x=0} \quad (1.15)$$

It must be stated that Equation 1.15 is valid also for a stirred solution because fluid velocity is almost zero at the electrode solution, due to the impenetrability of the electrode.

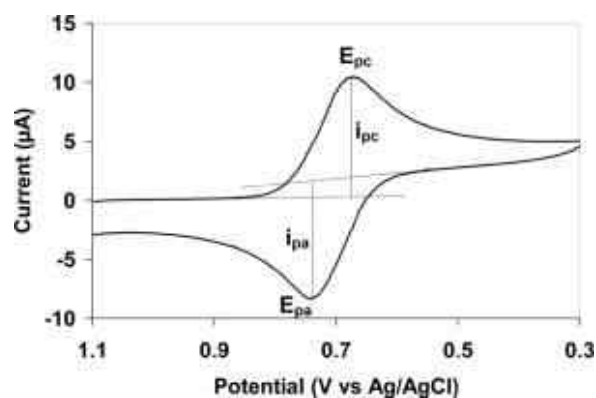
1.8.2 Cyclic Voltammetry

Cyclic voltammetry (CV) is a technique based on the application of a triangular wave potential to a stationary electrode called "working electrode" that is soaked into a non stirred solution. During this test, while considering the forward scan in Figure 10 (a), the potential starts negatively from a greater potential (point 1) to reach a lower value at the point 4. Point

4 is called switching potential and it is where there is enough voltage to cause a reduction or an oxidation of an analyte. In this case, from 1 to 4 reduction occurs, while oxidation is from 4 to 7. This cycle can be repeated with different values of scan rate [V/s], which is given by looking at the slope of Figure 10(a). The inversion of potential can be done numerous times during a single experiment to deeply study redox system, solid state chemistry and so on.



(a) Cyclic voltammetry excitation signal.



(b) Example of a cyclic voltammogram. Public domain image.

Figure 10: Cyclic voltammetry basics.

During a CV, the potential is measured between a reference electrode (it has a constant potential value), and a working electrode; current is calculated between the working electrode and a counter electrode. Thus, the resulting plot is similar to Figure 10 (b). This cyclic voltam-

mogram is a product that qualitatively describes the relationship between a great number of chemical and physical variables.

For each analyte that can be reduced or oxidized, while the potential varies, electrons are exchanged with the working electrode, hence there will be a variation in the measured current resulting into a peak in the voltammogram. If the process is reversible, when the voltage is switched and as soon as it reaches the value to reduce/oxidize the product formed during the first part of the scan, it will be produced a current of inverse polarity. This behavior is visible in the voltammogram because the new peak will have a similar shape of the latter, but it is inverted. From this plot, detailed information about reaction mechanisms, current densities, electron transfer kinetics and so on can be obtained. For example, if the analyte is in a solution, if the electron transfer is fast and this process is diffusion limited by species towards electrode's surface, it will result that the current intensity of the peak is proportional to the square root of the scan rate as described by Cottrell's equation (Equation 1.16).

$$i_p = 2.69 \cdot 10^5 A C n^{3/2} D^{1/2} v^{1/2} \quad (1.16)$$

This is valid for a solution at a temperature of 298,15 K; i_p is the peak current, A is the electrode area. C is the concentration, n is the amount of exchanged electrons, D is the diffusion coefficient and v is the scan rate. The current peak is proportional to the scan rate when diffusion is not limiting electron transfer as in case of electro active substances that are adsorbed on the surface of the electrode.

Again, it means that there is a deep relationship between changes in values of surface concentra-

tion and in the diffusion layer thickness: when the peak is achieved, the diffusion phenomenon is in control of the reaction; after the peak, the current drops independently from the applied potential, therefore it is explained why the forward and reversal current share the same shape. By using data from Figure 10 (b) it is possible to evaluate peak positions on the potential axis. These peaks are dependent on the electrochemical formal potential of the redox reaction. In Nernst's equation the potential is expressed by a constant value called 'standard potential' (E^0) while the other is variable and it is valid only for ideal solutions; to describe real solutions, concentrations are flanked by activities. The activity of an analyte is expressed by a coefficient which is constant for solutions belonging to the same type of analyte. Since the latter coefficients are constant, they can be included into the standard potential, thus it becomes 'formal potential'. From a CV, the formal potential for a reversible couple is computed as following:

$$E^0 = \frac{E_{p,anodic} + E_{p,cathodic}}{2} \quad (1.17)$$

Instead, the separation between the peaks is expressed by:

$$\Delta E_p = E_{p,a} - E_{p,c} = \frac{0.059}{n} [V] \quad (1.18)$$

For example, if the exchange involves only one electron ($n=1$), it means that the process has a peak distance of 59 mV. It must be underlined that both anodic and cathodic peak potentials are not dependent on the applied scan rate. Thus, Equation 1.18 can be exploited to compute n number of exchanged electrons, and using it into Equation 1.16 to determine the diffusion

coefficient D .

For every process involving more than a single electron exchange, the plotted cyclic voltammogram shows different and distinguishable peaks if the values of formal potentials E^0 are progressively higher for each singular step.

In Figure 11 [53] is it possible to observe various and separate reduction peaks from voltammo-

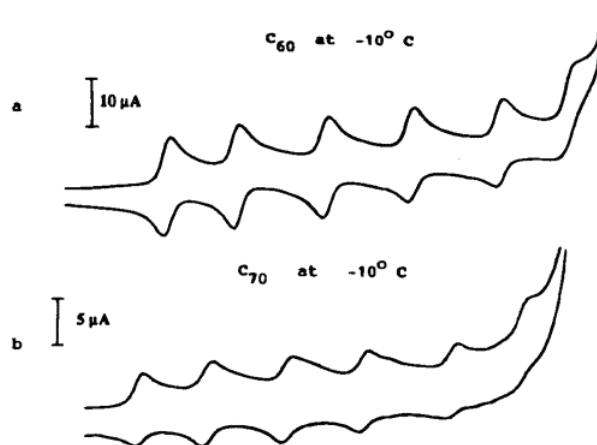


Figure 11: Examples of multi-electron reversible processes. Adapted with permission from [53]. Copyright 2016 American Chemical Society.

grams of (a) fullerene C_{60} and (b) fullerene C_{70} in an acetonitrile/toluene solution. This plot would be different if the redox process is conjugated to a chemical reaction as it happens for the most interesting - from a chemical point of view - non ideal processes.

The potential of an irreversible system is expressed by the following expression:

$$E_p = E^0 - \frac{RT}{\alpha n_a F} \left[0.78 - \ln \frac{k^0}{D^{\frac{1}{2}}} + \ln \left(\frac{\alpha n_a F \nu}{RT} \right)^{\frac{1}{2}} \right] \quad (1.19)$$

In Equation 1.19, R is the universal gas constant, T is the temperature, α is the transfer coefficient, n_a is the amount of electrons transferred during the charge step, while F is the Faraday's constant. For irreversible systems, a peak shift occurs with the scan rate: E_p is a value greater than E^0 because it depends on the overpotential which is affected by k^0 standard heterogeneous rate constant [cm/s] and α . However, this peak shift can be kept under control by varying the scan rate ν . In standard conditions, the half peak potential and the peak potential will be separated by $\frac{48}{\alpha n}$: as αn increases, the plot will be more narrowed. About the current peak, it is described by Equation 1.20:

$$i_p = 2.99 \cdot 10^5 n (\alpha n_a)^{1/2} A C D^{1/2} \nu^{1/2} \quad (1.20)$$

From the latter equation it is clear how concentration value still influences the current peak, but its effect is reduced by α . In a quasi reversible process, which has k^0 between 10^{-5} and 0.1 cm/s , current is affected by mass transport and also the charge transfer have k^0 between 10^{-5} and 0.1 cm/s ; its related CV plot is depending on $k^0 / \sqrt{\pi D n F \nu / RT}$, hence the more this expression decreases, the more the process is far from a reversible one. This basically happens at a very fast scan rate, hence with high values of ν .

1.8.3 Linear Sweep Voltammetry

Linear sweep voltammetry (LSV) is a voltammetric method involving the measurement of the current flowing through a working electrode while there is a variation of the potential applied to the analyzed solution. It is called linear because potential changes linearly over time. It is used for a stationary surface of an electrode (generally a solid one or a mercury drop electrode) and it can apply a higher scan rate, for conventional applications about dozen mV/s. In particular, potential is rapidly and linearly swept to a stationary electrode. The working electrode is the one in which reduction/oxidation occurs, hence it is the desired zone of studying. Then, there is the counter-electrode where, as the name may suggest, an opposite reaction from the one occurring at the working electrode takes place. From resulting plot is obtained an asymmetric peak which value is called current peak i_p . This peak has a value higher than the one obtainable from a slow scan: with faster scans the electron transfer becomes so rapid that it determines a quick call and an instantaneous discharge of all ions nearby the working electrode. Due to this ions depletion it is explicated how current peak decreases, almost collapsing, after a potential value called E_p ‘peak potential’. As a better clarification, it must be explained that with a slow scan the monitored current is only depending on species diffusion.

Figure 12 is very important because provides useful data about a reversible LSV wave. Firstly, the formal potential of the electrode E^0 is reached before E_p because the latter corresponds to a maximum in the concentration profile slope. Since concentration is proportional to this slope, current peak is used for computations. Secondly, it is clear how sharp is the current slope (in this case $n=1$): thus it is an immediate sign of a nernstian behavior. In addition, as stated

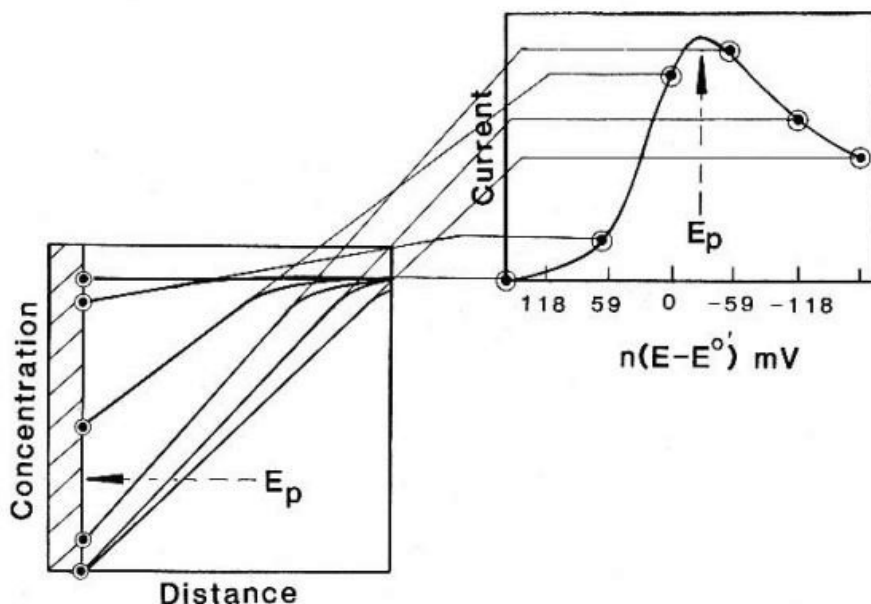


Figure 12: With such a quick scan rate, there is an increase of the slope of the concentration curve of a reversible steady-state LSV. Then, a rapid decrease occurs due to an expansion of the diffusion layer which causes the electrode surface concentration to change. As a result, current is maximum at E_p . Reprinted with permission from [51]. Copyright 2016 American Chemical Society.

previously, once E_p is measured, this serves as a good estimate of E^0 : it means that E_p provides an useful qualitative tool while giving quantitative information about thermodynamics of the redox couple.

Why is this wave-shape analysis so important? From Figure 13 it is immediate how the irreversible wave extends broader than the reversible case: the formal potential does not match $E_{1/2}$ because the latter is highly influenced by kinetics of electron transfer, thus its measure is not employed for qualitative analysis since it varies with the used experimental circumstances.

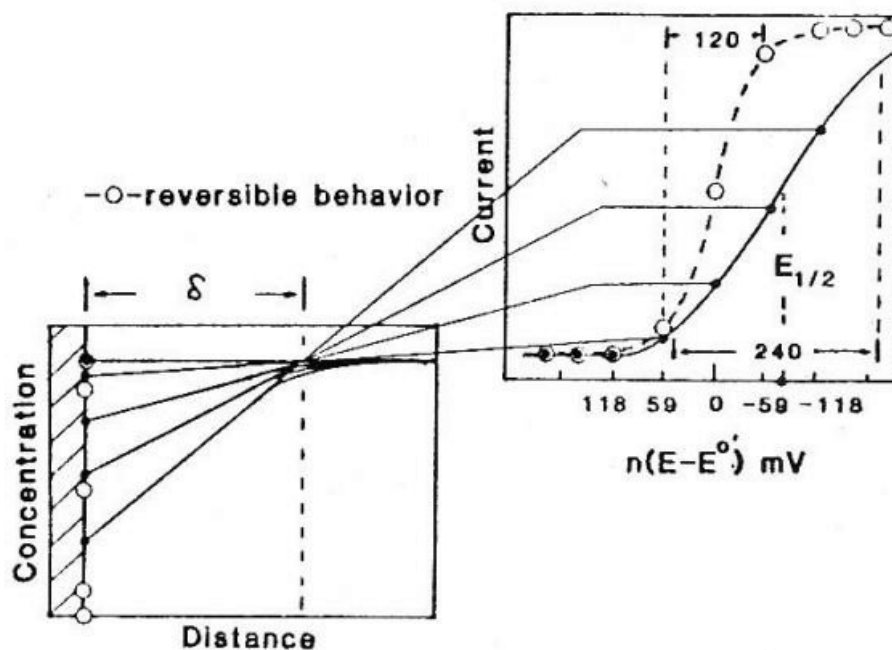


Figure 13: In this case the slope of the concentration curve is lower than the one of a reversible steady-state (white circles) since there is a sluggish kinetics of charge transfer. Thus, resulting boundary conditions are not nernstian. As a reminder, δ is the distance of the bulk concentration caused by convection phenomenon. Reprinted (adapted) with permission from ([51]). Copyright (2016) American Chemical Society.

Although limiting currents - needed for quantitative investigations - are measured at a negative potential, they are reached more difficultly as it occurs in the reversible case (it is a consequence of the reduced slope which suggests a failure to meet the nernstian behavior). This is due to a current response to the applied voltage which is slower than the one obtained from a reversible case.

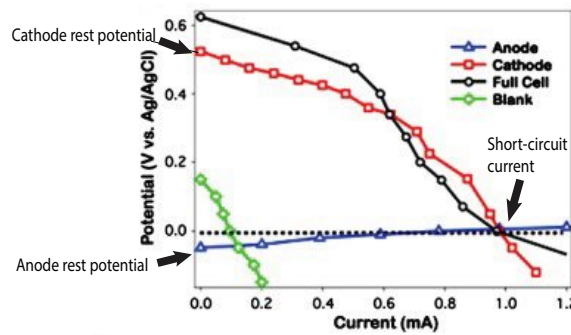
1.8.4 Open Circuit Measurements

From Ohm's law ($V=R*I$), the electric power is computed as $P [W]=V [V]*I [A]$: this means that, in order to evaluate the power output of a fuel cell, those two parameters are needed. The simplest way to perform this test is called 'open circuit potential' (OCP), in which the electrochemical potential is measured at open circuit (thus, current flowing is zero). In the past this test was carried out in a more rudimentary way with a voltmeter, but in this way it was not possible to acquire data about the kinetics of the cell. That is why a potentiostat is nowadays largely used. To perform an OCP test, the working and reference electrodes are connected and the potential difference across them is sampled as a function of time. The counter electrode is short-circuited from the external cell, hence no current flows through it, with the exception of the bias current of the measuring amplifiers, which is in the picoamperes range. If the measurement is performed using two electrodes with respect to another fuel cells electrode, the test is called 'open circuit voltage' (OCV). In this thesis, OCP tests were performed to retrieve the maximum voltage needed as an input for LSV tests.

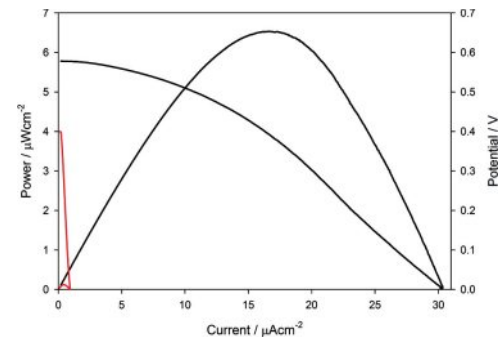
1.8.5 Polarization and Power Curves

Polarization curves are plotted in various ways. Firstly, they were determined employing galvanostatic test (because in the past it was enough simple and cheap to build a galvanostat than a potentiostat) like keeping a constant current to measure potential. Then, as far as more complex circuitry was being easy to build, potentiostats replaced galvanostats. As a result, polarization curves were traditionally plotted as potential values E versus current density i by performing a LSV with a very slow scan rate (about 1 mV/s). Their importance is such

that are used to study different contributing factors in the fuel cells like occurring reactions, concentration, activation potential and so on. In Figure 14 (a) [57] there is an example of polarization curves of an EFC anode, cathode and of the whole fuel cell. It has to be noted that the fuel cells plot is the sum of anode and cathode polarization plots. Its power is computed as the integral of voltage over current. After this analysis, the following step is to calculate power curves. Polarization curves can also be obtained exploiting various values of electrical resistors, measuring every time current and potential values. A power curve is a complementary



(a) Example of polarization curves. Adapted from Ref. 57. Copyright Elsevier.



(b) Power density is often plotted, preferred to power. Note that it is very unlikely that a real device operates at his best efficiency point during working conditions. Some researchers prefer to use voltage instead of current density as abscissa. Creative Commons Attribution License.

Figure 14: Examples of (a) polarization and (b) power curves.

plot deriving from polarization curve, hence it is common to find those two curves in the same

graph: they both share an equal x-axis with current density, while on the y-axis there is the derived power (or power density). In Figure 14 (b) [58] there are represented both power and polarization curves: in red regarding the first step of a two enzyme cascade, while in black a full six enzyme cascades

CHAPTER 2

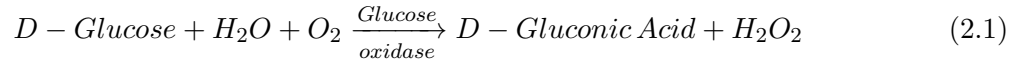
EXPERIMENTAL SETUP

The goal of this study is to understand and characterize the performances, limits and challenges of an enzymatic fuel cell. In particular, the main approach was to divide the work into two stages. First, purely electrochemical testing was performed to study the performances of the electrodes. Second, these electrodes were assembled in a microfluidic EFC and the device performance was characterized. The first stage aimed at observing the effects of enzyme immobilization, of the employed fuel/oxidant and the influence of its pH on the electrodes, as well as considering different materials or various coatings and explain the changes in the related properties; the second step was necessary for demonstrating the easiness and feasibility of a microfluidic system fabricated with novel advanced manufacturing techniques as a 3D-printing. Moreover, this latter was necessary to further study the enzyme stability, durability and the effect of fuel transport on the obtained electric power. The present chapter is structured to clearly explain and divide the used anodic and cathodic coatings, dealing with all the exploited materials and their properties. The last part is intended to provide informations about the accomplished microfluidic design and its realization.

2.1 Anode

2.1.1 Glucose Oxidase

Glucose oxidase (abbreviated: GOx) is an enzyme capable of catalyzing glucose ($C_6H_{12}O_6$) oxidation producing D-glucono- δ -lactone ($C_6H_{10}O_6$) and hydrogen peroxide as visible in Equation 2.1. Since it belongs to the oxido-reductase family, it means that this enzyme is able to enhance the electron transfer from the an electron donor (D) to an electron donor acceptor (A) $D + A \longrightarrow D + A$. Hence, it is classified as EC 1.1.3.4tab:PAFCmaterials, because 'EC 1.1.3' stands for all oxido-reductases which have oxygen as electron acceptor, while acting on CH-OH groups from the donor.



GOx is a natural product of certain insects and fungi, in particular where its product H_2O_2 is needed as an anti-bacteria and anti-fungi when glucose and oxygen are both present [59]. Usually GOx is extracted from *Aspergillus niger* since 1928 [60], which is a fungus very common in an indoor environment, capable of causing black mould on some vegetables and fruits. Despite this, GOx is considered safe, and it has been employed in a large variety of environments: as a liquid additive [61] for food industry to preserve or as an antioxidant. It may seem strange, but it is used in bread production to guarantee a better texture [62] as replacing the carcinogen potassium bromate ($KBrO_3$) to oxidate two proteins of flour and create additional bonds while gluten is generated [63]. Another good example of the versatility of GOx can be found

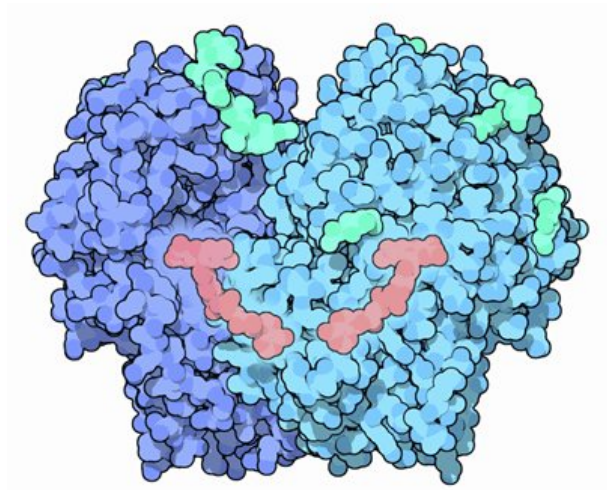


Figure 15: Glucose oxidase represented: dark and light blue for its subunits, pink for FAD. Creative Commons Attribution License.

in nature [64]: GOx and glucose will endlessly produce hydrogen peroxide, which is needed for the lactoperoxidase system. This latter belongs to the immune system, and it requires a contemporaneously presence of three components, as the hydrogen peroxide, to be activated for anti microbial aims. As represented in Figure 15, GOx is a dimeric (thus a macromolecular structure formed by non covalently bound macromolecules) protein: in particular, it is homodimeric due to twins subunits and a equal couple of flavin adenine dinucleotides (FAD). A FAD is a prosthetic group, which in turn is a covalently bound cofactor. It must be specified that in biochemistry it is defined 'cofactor' a non-protein chemical compound needed to the activity of a protein, usually enzymes. It was demonstrated that FAD allows electron transfer during GOx activity [65].

When FAD (Figure 16) is in its quinone variant (oxidized form), it means it is capable to accept

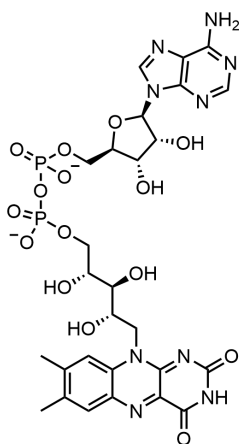


Figure 16: Flavin adenine dinucleotide (FAD) constitution. Creative Commons Attribution License.

two protons and two electrons to become hydroquinone ($FADH_2$, reduced form) as instructed in Figure 8. As a reminder, a quinone is an organic compound which comes from aromatic compounds (e.g. benzene) after that an even number of $-CH=$ groups turns into $-C(=O)-$, without any successive swap of double bonds [66]. The most employed GOx comes from *Aspergillus niger*, and among its composition there is about 17 wt.% of carbohydrate (which in turn is made of 80 wt.% of N- or O- glycosidically linked mannose; a glycosidic linkage is a covalent bond between a carbohydrate (sugar) to another group) and about 20% of amino sugar (2-amino-2-deoxysugar) [67; 68].

GOx is particularly interesting due to its electrochemical properties that are tried to be exploited for fuel cells applications or as glucose sensor. In this thesis, GOx from *Aspergillus niger* (EC 1.1.3.4) was ordered from Sigma-Aldrich (#9001-37-0).

2.1.2 Hexylferrocenyl-LPEI (Fc-C₆-LPEI)

Following a trend started 20-25 years ago [69], a lot of accomplishments have been reached about the discovery and studies on electroactive polymers. These materials have been put forwards due to a will to deeply understand the kinetics and fabrication of surface films: it must be underlined how vast is the field of possible applications of electroactive polymers for corrosion phenomena, bioelectrochemistry and so on. Because of the easiness of controlling a redox process, plus the reversibility of that redox process in these polymeric materials, the latter are vastly employed to design electrochemical and microelectronic devices as biosensors, batteries or biofuel cells [70]. A redox polymer exhibits an alteration of its electrochemical properties caused by electron gain/deprivation (hence, for IUPAC there must be a reversible reduction/oxidation phenomenon within the polymer groups). The above mentioned groups can be electro-statically bound, covalently or directly attached within the polymer backbone, which is the main series of covalently bounded atoms representing the continuous skeleton of the molecule. Historically, ferrocene side groups were incorporated as side groups of a redox polymer for their organometallic redox half; it was exploited as micro/nano particles or as copolymers. By playing with factors as nature of the polymer backbone or with the location and distance between localized redox sites it is possible to achieve a broad range of results. It must be reminded that in chemistry a system is defined 'conjugated' when there are p-orbitals linked with delocalized electrons in molecules, for example with a sigma bond (the strongest covalent link): as a result single and multiple bonds are alternating. The delocalized π -electrons come from the bridging of interjacent bonds, hence they come from all the adjacent aligned

p-orbitals. Just to provide a clear example of how all these variables affect the electron transfer, if a polymer has multiple redox groups (and/or conjugated main chain) the electron transfer occurs in form of jumps among the redox centers or a semiconjugated main chain. By observing all the parameters of a redox process, it is possible to correlate the latter to the properties of the examined polymer. The used redox polymer which has been chosen for this experiment is hexylferrocenyl-LPEI (Fc- C_6 -LPEI): it was demonstrated [71] that a higher tether length was positively affecting the electron transfer and the GOx response, yielding a working time of about 40 hours and current densities of $1000 \mu A/cm^2$. Moreover, this linear poly(ethylenimine) based redox polymer was very stable in conditions of coupled high pH level (Figure 17) and with dibasic phosphate, which was not so predicable judging from some previous research [72; 73; 74]. This is a result of the extension of the ferrocene group in addition to the longer tether caused by C_6 .

The voltammogram peaks typical of a multiwave redox process were removed thanks to the extension of the ferrocene groups from the LPEI main chain. Coupled with the GOx enzyme, and adding 0.1 M of glucose (value for which the redox polymer achieves the maximum current den-

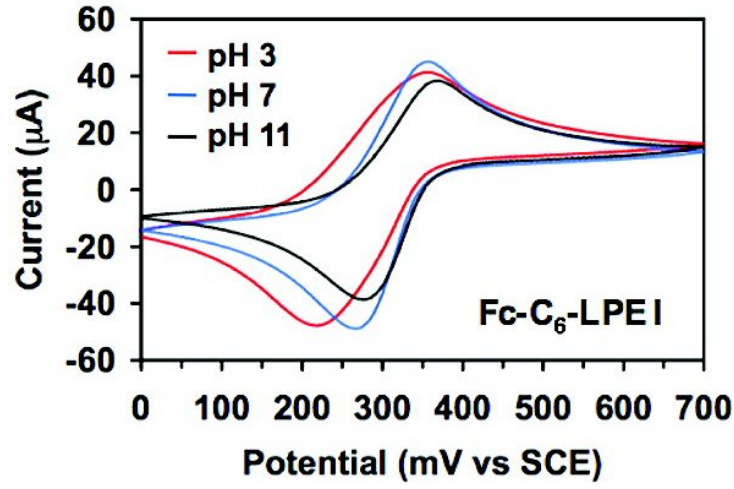
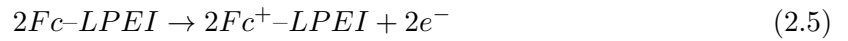
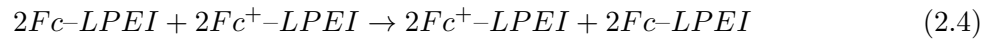
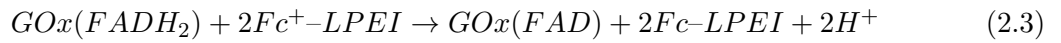
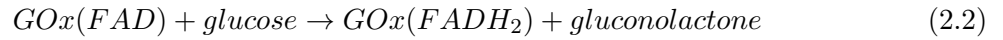


Figure 17: CVs of cross-linked films of $\text{Fc-C}_6\text{-LPEI}$ with different pH levels of phosphate buffered saline (PBS). Reprinted with permission from [71]. Copyright 2016 American Chemical Society.

sity, as outlined by Figure 18) to a neutral pH PBS , there are the following reactions occurring:



It means that from Equation 2.2 there are two electrons moving from glucose to GOx which, after being reduced in FADH_2 form, will relocate electrons to the ferrocenium (which comes from the oxidation of ferrocene) redox centers (Equation 2.3). After this, electrons are trans-

ferred within ferrocene and ferrocenium centers (Equation 2.4). In the end, the electrode surface receives electrons coming from Equation 2.5.

In this work, hexylferrocenyl-LPEI was prepared following the main instructions reported in

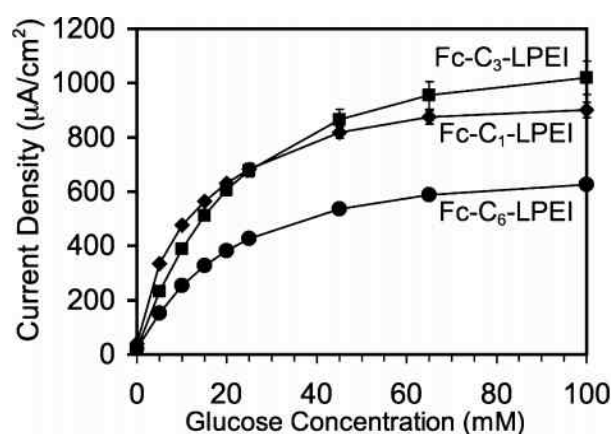


Figure 18: Glucose concentration effects on redox polymers. Fc-C₁-LPEI, Fc-C₃-LPEI, and Fc-C₆-LPEI (all coupled with GOx) curves are plotted. It was said that increasing the space between redox centers and polymer main chain causes an increment of the volume that can be processed by redox centers, thus yielding to an enhanced electron transfer and enzymatic response [75] [76]. However Fc-C₆-LPEI exhibits lower maximum current density than the other redox polymers, which means there are other factors that must be investigated. Reprinted with permission from [71]. Copyright 2016 American Chemical Society.

Ref. [71] and Ref. [77]. Linear polyethylenimine (LPEI) was ordered from Polysciences, Inc. It was chosen to order a commercially available LPEI with a molecular weight of 100000 in order to be as close as possible to the LPEI from Ref. [77], which in turn was characterized by a MW~ 86000. (6-Bromohexyl)ferrocene, methanol, acetonitrile and diethyl ether were

purchased from Sigma-Aldrich. Firstly, a cloudy mixture was formed in a round flask with a reflux condenser using 10 mL of acetonitrile with 300 mg of LPEI, and then heated for about 15 minutes to reflux solvent. The mixture became clear by adding 2 mL of methanol, then 380 mg of (6-Bromohexyl)ferrocene were injected. After a night in which the solvent was refluxed by heat and removed under pressure, diethyl ether was added for the removal of impurities. The final mixture yielded about 650 mg of hexylferrocenyl-LPEI (Figure 19).

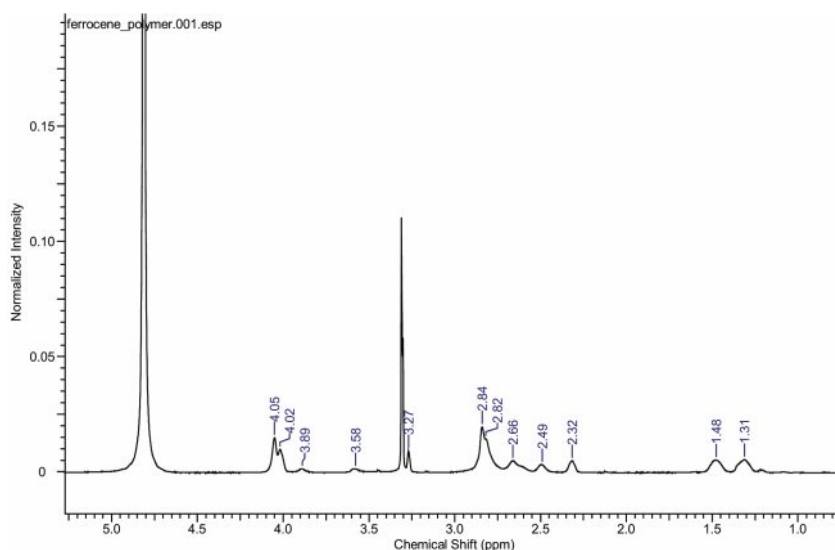


Figure 19: ^1H NMR spectrum of hexylferrocenyl-LPEI. The obtained peaks are not perfectly overlapping the ones described in [71], probably due to the usage of a commercially available LPEI slightly different from the one produced in the reference paper.

2.1.3 Ethylene Glycol Diglycidyl Ether (EGDGE)

Ethylene glycol diglycidyl ether (EGDGE, Figure 20) is a crosslinker for carboxyl, amine and hydroxyl functional polymers. Thanks to its water solubility it is employed in a broad range of fields, also for biomaterial applications [50].

In general, a crosslinker is a molecule with at least two reactive extremities which make it

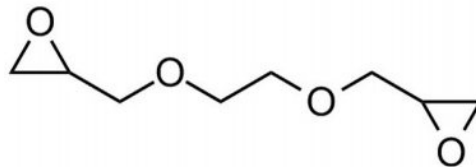


Figure 20: EGDGE structural formula.

capable of attaching to certain functional groups by a covalent bond. This is a technique called bioconjugation if usage has been done with bio molecules such as proteins. Crosslinking is the main key to create sensors for ELISA utilization (due to an enhancement of the resistance to dissolution in aqueous solutions) and to study proteins behavior. Crosslinking is also used in rubber industry during vulcanization process to enhance the elasticity of tires. Useful tests to measure the degree of crosslinking are part of the swelling experiments: after soaking the crosslinked film/sample into a good solvent at a well defined temperature, measurements are taken to observe if volume/mass changes occur. A good crosslinker exhibits less swelling. The

ASTM F2214 prescribes to measure how much the height of the sample changes, to relate it to a volumetric change. In order to compute the degree of crosslinking, Flory's Network Theory [78] has to be used since it correlates the solvent's density with the Flory Interaction Parameter -of the solvent interacting with the examined specimen-. For this thesis, EGDGE was ordered from Polysciences, Inc.

2.1.4 Anode Coating

In order to coat a bioanode of 6 cm^2 , the following steps have been followed according to a published research [79]: dissolve the hexylferrocenyl-LPEI polymer in deionized water, respecting a ratio of 10 mg/mL to obtain 210 μL of polymer solution. Prepare 90 μL of GOx solution, following a ratio of 10 mg of GOx into 1 mL of DI water. Pick 11.25 μL of EGDGE solution, in which 10% v/v has to be respected. The three obtained solutions were mixed together and vortexed for 20 seconds, then the enzymatic redox gel was ready to be casted on the electrode surface. About 50 $\mu\text{L}/\text{cm}^2$ were drop casted using a pipette to facilitate the coating, and the electrode was dried under room temperature for less than 24 hours. In Figure 21 it is possible to observe the final result after the enzymatic redox gel coating. It has to be reminded that six anodes. In this case, the substrate used was Toray paper 060 non-wet proof, which was previously waxed at the extremities to obtain 1 cm^2 of free surface each. These anodes were used for electrochemical tests, but the used ratios were employed for the final design of the microfluidic EFC.

To evaluate further characteristics of the coating gel, additional CVs were performed. In particular, ratio were changed to have 8 mg/mL of both polymer solution and GOx solution, while

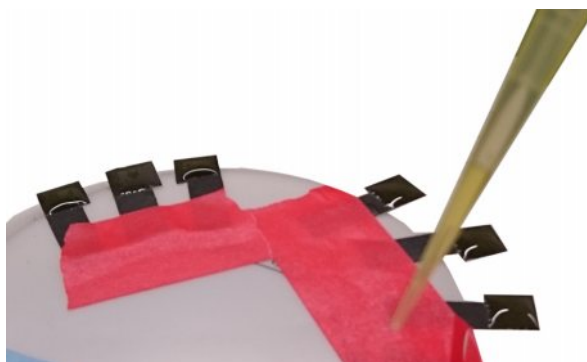


Figure 21: Enzymatic redox gel drop casted on six anodes. In this case, the substrate used was Toray paper 060 non-wet proof, which was previously waxed at the extremities to obtain 1 cm^2 of free surface each. These anodes were used for electrochemical tests, but the used ratios were employed for the final design of the microfluidic EFC.

the EGDGE solution was increased to have 20% v/v ratio. The main hypothesis behind those decisions is to compare the performances of the two coatings, and the result expected is a not important decrease of anodic peak current despite a reduction of 20% of the used polymer and enzyme. On the other hand, the crosslinker volume ratio was increased to try counterbalancing the previously mentioned decreased proportions.

2.2 Cathode

2.2.1 Bilirubin Oxidase and Laccase

For what concerns the cathode coating, the employed enzymes belong to the multicopper oxidase (MCO) family. MCO are enzymes capable of oxidizing their substrate by transferring electrons to a trinuclear copper center called TNC (made of the type 2 T2 and the binuclear type 3 T3) after having received them at a mononuclear copper nucleus -type 1 T1-. O_2 is linked

to the T2 and, after a four electrons exchange, it is transformed into water [80]. MCOs are characterized by 2, 3 or 6 of these nuclei, and they are largely used for EFC applications due to their great stability and high redox potential during oxygen reduction reaction (ORR). Enzymes belonging to this family are very numerous and easily found in sources as fungi, bacteria, green plants and animals. This, plus the fact that nowadays a wide range of engineering techniques exist to produce MCOs, has to be considered for the determination of a common base for enzyme testing.

Bilirubin oxidase (BOd, classified as EC 1.3.3.5) is an enzyme catalyzing the reaction $2\text{bilirubin} + O_2 \rightleftharpoons 2\text{biliverdin} + 2H_2O$, which is the oxidation of a tetrapyrrole, that is a group of compounds made of four pyrroles C_4H_5N linked by covalent (EC 1.3.3.5 bonds or by one carbon bridge. BOd activity is in its best efficiency range if the employed solution is within a pH range from 6.0 to 8.0 [81]. Studies [82; 83] confirmed that BOd is capable of being used as a cathode without the intermediate production of H_2O_2 : therefore, its ORR involves an exchange of four electrons (in Table VIII are explained the possible ways of electron transfer for BOd). For this work, BOd was purchased from Amano and used as received in its light blue to yellow powdered form.

Laccase (from *Trametes versicolor*, EC EC 1.10.3.2, Figure 22) is the most studied and employed MCO enzyme due to its historical heritage, largely coming from its good turnover number and thermostability. Laccase activity is at its best efficiency if the employed solution is within a pH range from 4.0 to 5.5. For this work, laccase was purchased from Sigma-Aldrich and used as received in its light brown powder.

TABLE VIII: BOD REACTION

Reaction	Potential
$O_2 + 4H^+ + 4e \longrightarrow 2H_2O$	1.23 V vs. NHE
$O_2 + 2H^+ + 2e \longrightarrow H_2O_2$	0.68 V vs. NHE
$H_2O_2 + 2H^+ + 2e \longrightarrow H_2O$	1.77 V vs. NHE

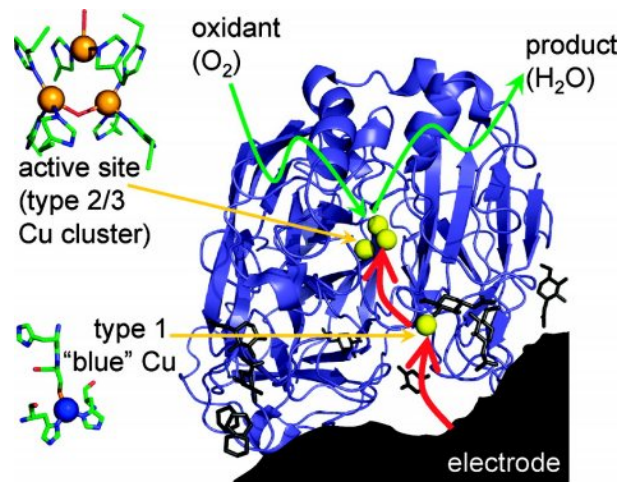


Figure 22: Laccase from *Trametes versicolor* represented: blue for the protein superstructures, yellow for the copper nuclei. Reprinted with permission from [84]. Copyright 2016 American Chemical Society.

2.2.2 TBAB-Nafion

Nafion is a material invented about fifty years ago by DuPont [85]. Basically, it is a fluoropolymer based on sulfonated tetrafluoroethylene which groups characterize its ionic properties [86] (Figure 23). Originally employed for fuel cells applications in form of a membrane permeable to protons exchange going from sulfonic acid SO_3H , then it witnessed a period in which

interest has risen towards its modification through the exploit of a recast process.

Nafion has been used as an electrode coating for enhancing their performances, stability and

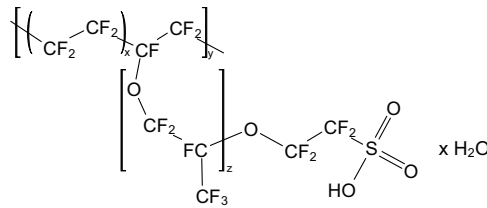


Figure 23: Nafion structural formula.

sensitivity. This latter is a property which is directly linked to the amount of generated output from a sensor/fuel cell; among the various available methods to increase this parameter, there is the use of micelles-shaped structures within a polymeric membrane. A higher amount of micelles and/or an increase in their size corresponds to an increased mass transport, thus ions diffusion is boosted; the latter size increment can be obtained by stepping up the hydrophobic property of the Nafion polymer. A possible valid solution was previously found [87] by modifying with salt a Nafion solution, because an excess of hydrophobic alkyl ammonium salt increase the size of Nafion micelles due to a replacement of the protons (by the ammonium cations) from the sulfonates on the side of the polymer [88]. Following a path indicated by recent research [89] that started with Ref. [90], in this thesis a Nafion solution (1100EW, 5 wt.% in lower aliphatic alcohols with 15-20% water) was modified with tetrabutylammonium

bromide (TBAB). By respecting the ratio of 39.19 mg of TBAB in a mL of Nafion suspension, keeping in mind that it was important to avoid casting more than $1 \text{ mL} / 8 \text{ cm}^2$, about 2.36 mL of TBAB-modified suspension were prepared after 20 minutes of vortexing. This latter amount was computed in order to respect the previously mentioned casting ratio for the used weighing boat as a casting surface (Figure 24(a)). The mixture was left to dry for 24 hours in a low humidity environment, which humidity value was kept under control by a continuously working dehumidifier.

Then, the dried film was soaked for 24 hours in a $14.7 \text{ M}\Omega$ DI water to allow the removal of

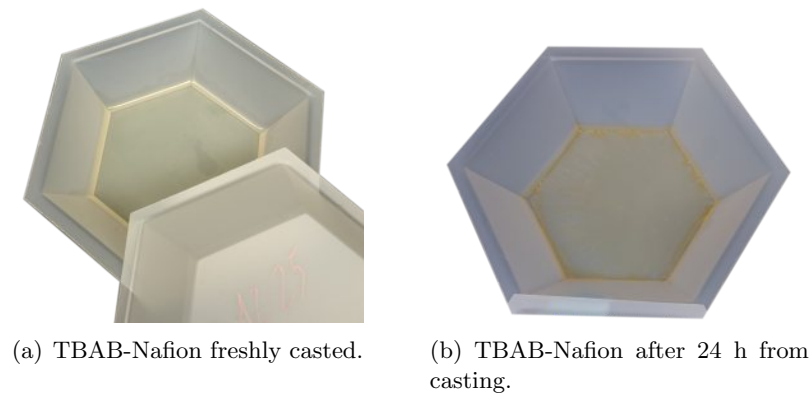


Figure 24: First steps of preparing TBAB-Nafion.

excess salt. A good indicator was the self-peeling of the film from the weighing bowl surface, almost without any breaking. After this point, the film was rinsed thrice with $14.7 \text{ M}\Omega$ DI water

and successively it was left to dry. Finally, the opaque dried pieces were transferred in a glass vial and suspended with ethanol (indicative ratio: 1 mL of ethanol for 5 mL of TBAB-Nafion casted solution).

2.2.3 Multi Walled Carbon Nanotubes

Multi walled carbon nanotubes (MWCNTs) are a sub-group of carbon nanotubes, which in turn are allotropic forms of carbon characterized by a cylindrical shaped nanostructure. Thanks to some of their properties, like thermal/electrical conductivity, they have rapidly become interesting from both a researching point of view and an engineering one. Carbon nanotubes are allotropic form of carbon with a cylindrical nanostructure. Their name is due to the presence of at least two walls each of them thick about one atom and rolled inside each others, as it happens when two or more sheets are rolled like a parchment thanks to Van der Waals forces (Figure 25).

Instead of using 2,2'-azino-bis(3-ethylbenzothiazoline-6-sulphonic acid) (ABTS), MWCNTs are

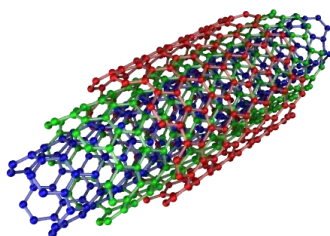


Figure 25: MWCNTs representation. Creative Commons Attribution License.

necessary to achieve direct electron transfer for the cathode. Usually, all that is needed is to use a commercially available solution as the one provided by CheapTubes.com, which allows the choice of various parameter like the diameter, the wanted loading and the functional groups linked to the ends/sidewalls of structure of carbon nanotubes. Functionalization of nanotubes is a chemical method that can be achieved in two ways: by directly attaching the desired functional groups to the graphitic surface; or by employing nanotube-bound carboxylic acids [91; 92]. In previously EFC published papers, there is a vast employment of hydroxyl (OH) functionalized carbon nanotube, both as single or multi, in powder or liquid form. Nevertheless, based on the research paper [93] and as depicted in Figure 26, it was chosen to employ anthracene modified MWCNTs (Ac-MWCNTs) to have enhanced DET, since anthracene boosts the link between substrate of the electrode and T1 nucleus of the employed MCO [94]. In this work, the

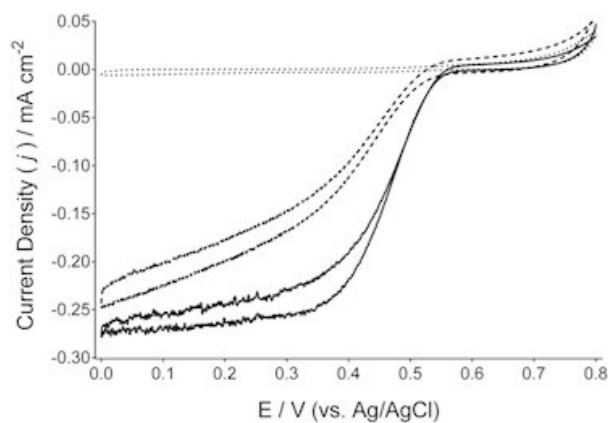


Figure 26: Performance differences between BOd based cathode, including OH-MWCNTs (dashed plot) and Ac-MWCNTs (solid plot). R. D. Milton [93]. Reproduced by permission of The Royal Society of Chemistry.

used anthracene modified MWCNTs are a gift from Dr. Shelley Minteer's Research Group (University of Utah, Salt Lake City).

2.2.4 Cathode Coating

A long series of electrochemical tests were performed on various substrates of 1 cm^2 to evaluate the performances of the coating mix, of the different enzymes, of the used solution and for the coupling with the anode. Tests were performed on both toray paper and buckypaper, and to evaluate the differences achieved with MET and DET. In particular, the starting point of this analysis is a previously published coating procedure. To be specific, to coat 3 cm^2 of substrate it was necessary to mix 1.5 mg of enzyme in $75\text{ }\mu\text{L}$ of 0.2 M citrate/phosphate buffer (pH 7 when the measured grams were of BOD; pH 5 if the picked quantity was of laccase). Then, 7.5 mg of Ac-MWCNTs were added to this solution by vortexing for a minute, and sonicating for 15 seconds. This step was successively repeated other three times. After this, $25\text{ }\mu\text{L}$ of TBAB-Nafion were added. It followed another cycle of mixing and sonicating with the same times previously reported. Finally, the obtained mixture (very similar to an ink) was coated on each previously prepared surface through the use of a brush.

2.3 Design

In order to study the performance, life and stability properties of a working microfluidic enzymatic fuel cell, the designed structure entails the use of a flooded cathode and anode. In particular, both coatings were performed on a Toray paper 060 non wet proof (purchased from FuelCellEarth) as a substrate, for a final active surface of 6 cm^2 per electrode, respecting the previously reported ratios. All the three parts were designed using Solidworks 2015, and 3D

printed by a stereolithography based 3D printer [95], model Form 1+ from Formlabs (Fig. 27 (a)). The employed material is a clear resin, able to be cured with a final resolution of $25\text{ }\mu\text{m}$ per layer, with a good bio-compatibility.

Titanium wires were inserted into each base in order that contact between each of them and

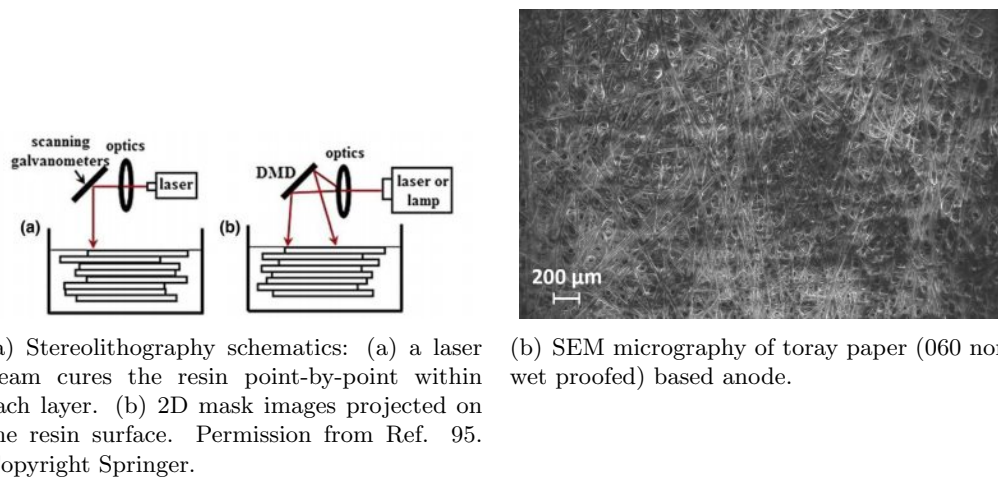


Figure 27: Some of the used techniques and equipment.

its related electrode is constantly assured by mechanical interference. The final system was assembled by four bolted joint after that two microfluidic 1/16" luer locks, one as an inlet and one as outlet. The provided solution, pumped with a Nexus 3000 syringe pump, was a pH 7.0 citrate/phosphate buffer with 0.1 M glucose which has been previously saturated with oxygen (from Praxair OX 4.3UH-T). For reasons already described in the former sections, the nature

of the chosen microfluidic design (one inlet) sets the choice of a pH level suitable for both anode and cathode at the same time. Since GOx has an optimum behavior for a pH between 6 and 8, BOD was selected as a MCO enzyme for the cathodic coating.

As a further solution to prevent leakage, a silicon based glue was used to seal the walls of the final assembly (Figure 28).

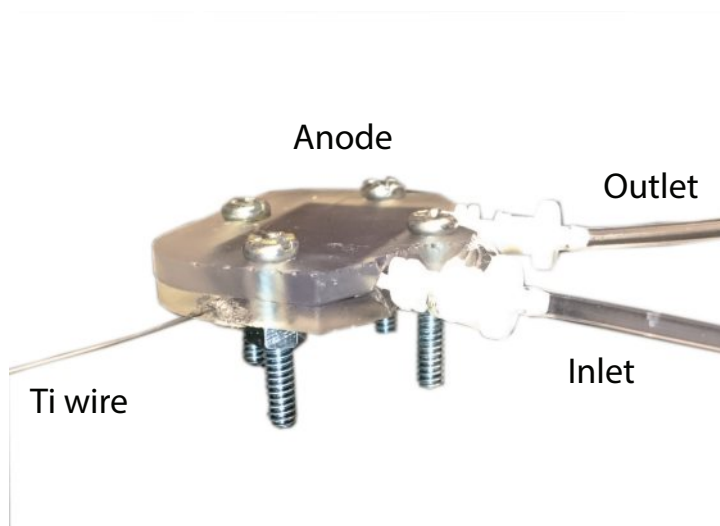


Figure 28: Photo of the final microfluidic EFC.

CHAPTER 3

RESULTS AND DISCUSSION

The goal of this chapter is to develop a comprehensive evaluation regarding the performances of a microfluidic enzymatic fuel cell. In particular, several tests have been carried out in order to have an exhaustive understanding of the electrochemical reactions occurring into the final assembly. Each result is afterward presented and discussed, taking into account comparative achievements of other experimental publications. As a reminder, all the electrochemical tests (CVs, OCPs, LSVs) have been performed with a CH 630E purchased from CH Instrument and operated with a saturated calomel electrode (SCE, purchased from CH Instrument) as a reference electrode and with a custom made platinum mesh as a counter electrode (99.9% Pt, mesh 52, resistivity $10.6 \mu\Omega\text{-cm}$, purchased from Sigma-Aldrich).

3.1 Anode

In order to characterize the GOx-based anode performances, several electrochemical tests were performed as previously indicated in 2.1.4. Initially, CVs have been performed to have a comparative parameter with Ref. [94]. In this case, the employed hexylferrocenyl-LPEI (Fc- C_6 -LPEI) has been synthesized as in Ref. [71]. I acknowledge Dr. Shelley Minteer's Research Group for providing the initial quantity of the needed redox polymer.

The aim of Figure 29 is to provide a good evaluation method about the quality of the used coating: in particular, what is important to underline is how the variant of hexylferrocenyl-

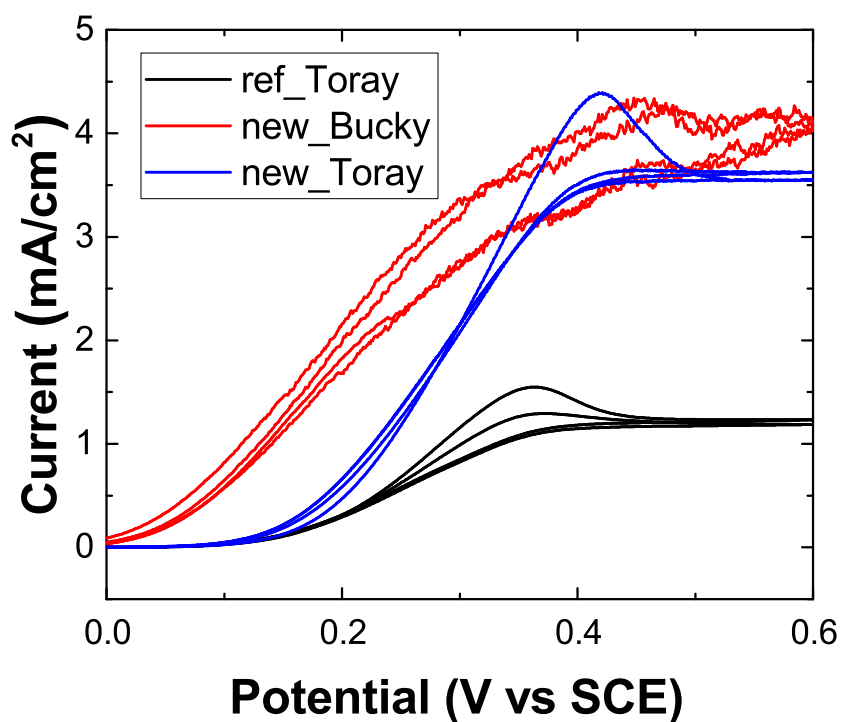


Figure 29: Cyclic voltammograms of the redox hydro-gel used to coat the anode. The reference polymer, coated on toray paper as indicated in 2.1.4, is represented by a black solid curve. The variant and heavier polymer was tested on both toray paper and buckypaper, respectively represented by blue solid curve and red solid line. As usual, same instructions indicated in 2.1.4 have been applied. Tests were carried within a stirred 0.2 M citrate/phosphate buffer solution with 0.1 M of glucose, at pH 7. Scan rate of 1 mV/s, at temperature of 26 °C.

LPEI prepared in the lab (blue and red solid lines; synthesized as described previously in 2.1.2) performs better than the one reported in Ref. [71] (black solid line). Considering the same substrate -toray paper-, it is quite visible how the heavier hexylferrocenyl-LPEI helps to reach a peak at least three fold higher than the one achieved by 'standard' Fc- C_6 -LPEI: despite the right shift towards higher potential values, it reached a value of 3.5 mA/cm^2 . Although in

Figure 29 plots are referred to different substrates, the previously mentioned results have been confirmed also on buckypaper. In this case, an almost equal anodic current peak was reached at about the same potential value, except that its trend (red solid line) is not as smooth as in the toray experiments. This difference among the different behavior of these two substrates is due to their intrinsic and unlike structure: since buckypaper substrate is an aggregation of carbon nanotubes, its morphology is affected, presenting similarities to a sponge. This is a factor which was also influencing the coating: if toray paper showed a quasi immediate absorption of the deposited redox gel, buckypaper was harder to cover. In particular, while ejecting the coating solution from an adjustable volume pipette, the droplets were macro aggregating and it was almost impossible to clothe all the free area of the electrode. This is certainly due to a high amount of multi walled carbon nanotubes which were blend in the substrate during the fabrication process of the buckypaper.

After the achievement of the above mentioned results, it was hypothesized that an important decrease of the polymer and GOx quantity should not severely affect the anodic performances of both toray paper and buckypaper. After a reduction of 20% of both polymer and GOx ratio (down to 8 mg/mL instead of 10 mg/mL), coupled with an increase of EGDGE proportion (20 % v/v ratio), resulting plots were obtained in Figure 30. This time both peaks are shifted towards mid values of potential (around 0.3 V), with outputs of, respectively, 2.1 mA/cm^2 and 2.8 mA/cm^2 . In this case, toray paper was the most affected substrate from the ratios reduction; nevertheless, the output is still higher -almost the double- than the current density achieved in Ref. [94]. Among the main reasons, it is hypothesized that this is due to a longer

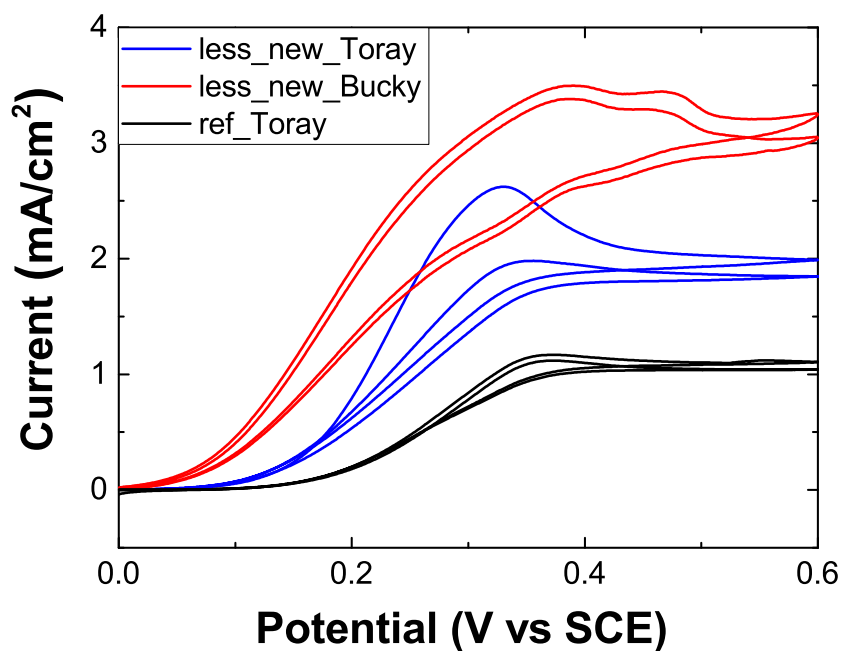
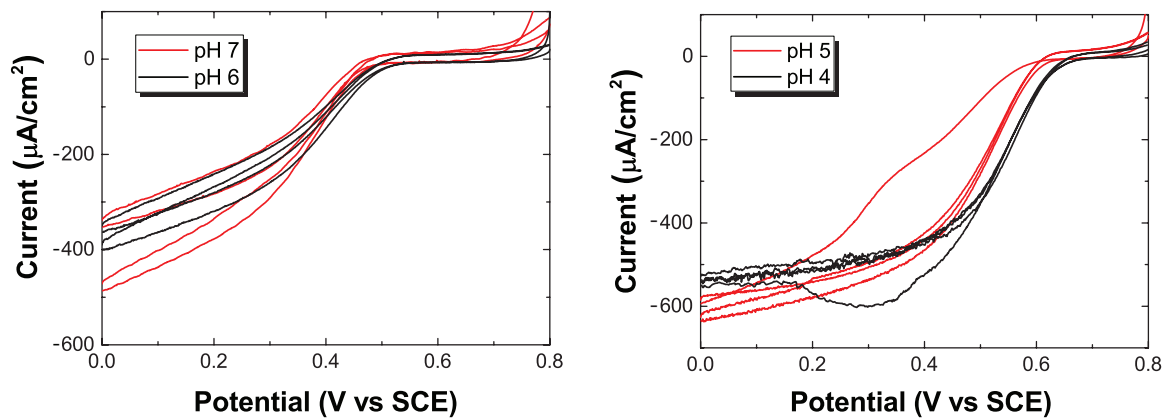


Figure 30: CVs of the original anodic coating with the reference polymer on toray paper (black solid line) and a light version, but with the new heavier polymer. In particular, for both toray paper (blue solid line) and buckypaper (red solid line), the coating employed 20% less of both -the heavier- polymer and GOx quantity. All CVs were carried within a stirred 0.2 M citrate/phosphate buffer solution with 0.1 M of glucose, at a scan rate of 1 mV/s and temperature of 26 °C.

polymer backbone chain: in fact, the variant Fc- C_6 -LPEI is based on a longer LPEI than the one synthesized in the reference paper (100,000 vs about 86,000). This means that there are more redox sites available to the ferrocene and therefore to the GOx. Moreover, this self produced redox polymer has the further advantages to eliminate preparatory steps needed for the LPEI synthesis, which is not an expensive product and it comes available with different molecular weight options.

3.2 Cathode

The aim of this thesis is to characterize the performances of a fully enzymatic fuel cell, thus it is clear the importance of the chosen cathodic coating. As described in 2.2.1, the possible paths to follow involve the usage of bilirubin oxidase or laccase. However the selected coating, which has been reported and documented in 2.2.4, is based on DET mechanism between the MCO enzyme and its substrate. In the upcoming figures it is possible to evaluate the reduction of oxygen by the above mentioned MCOs, and how their behavior is related to the pH level of the analyte. For example, in Fig. 31(a) is it visible how the onset potential of the



(a) Cyclic voltammograms of a BOD based cathode on toray paper 060, non wet proofed. CV performed at pH 7 (red solid line) and pH 6 (black solid line).

(b) Cyclic voltammograms of a laccase based cathode on toray paper 060, non wet proofed. CVs performed at pH 5 (red solid line) and pH 4 (black solid line).

Figure 31: Comparison of BOD and laccase based cathodes, within different pH values selected within the range of optimum pH for each enzyme. All CVs were carried using a 0.2 M citrate/phosphate buffer solution oxygen saturated, at a scan rate of 1 mV/s and temperature of 26 °C.

oxygen reduction occurs at about 0.5 V (vs SCE), yielding a catalytic current between 0.37 and 0.5 mA/cm^2 . The performed CVs highlight how BOx based DET coating exhibits a better enzymatic response with a pH value closer to the defined physiological one. On the other hand, for what concerns Fig. 31(b), this pH dependency is less evident: laccase based DET coating more or less follows the same behavior in a buffer of pH 5 and 4. With respect of BOx, laccase starts to reduce oxygen at higher values: the onset potential is 0.59 V for a pH 4 buffer and 0.50 V for pH 5 buffer. Moreover, laccase based coating displays higher catalytic current values than the bilirubin oxidase one, due to its capability of reaching at least 0.53 mA/cm^2 , with peaks of 0.61 mA/cm^2 . After achieving the above presented results, the following step

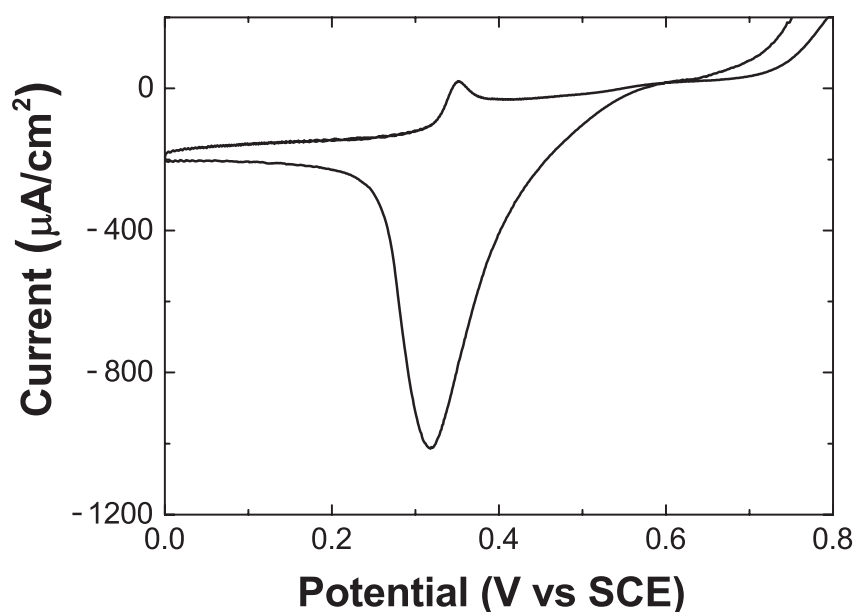


Figure 32: Investigation on a MET laccase cathode. CV performed with a pH 4.5 0.2 M citrate/phosphate buffer solution oxygen saturated, at a scan rate of 1 mV/s and temperature of 25 °C.

of this work was to further broaden and explain the available choices and the recurring issue while designing an enzymatic fuel cell. By comparing the order of magnitude between the measured anodic and cathodic catalytic currents, it is straight forward that it is the cathode which will limit the EFC performance. In the best case, even by employing for instance a DET laccase coating on a non wet proofed toray paper, it will yield a current peak six times lower than the one reached in Figure 29. From this point of view it was necessary to consider a MET coating: the only difference from the process presented in 2.2.4 is the substitution of anthracene modified MWCNTs with the mediator ABTS. This time, the detected peak occurred at 0.32 V, showing a density of 0.9 mA/cm^2 (Figure 32), higher than before because the mediator helps to link the deep buried active sites of an enzyme to the substrate, facilitating the electron transfer. Despite an increase of 47% with respect of the DET case, this outcome is still three times lower than the anodic current. On the other hand, as suggested by the shape of the CV in Figure 32, after the peak MET presents lower current values with respect of a DET laccase cathode: respectively about 0.22 mA/cm^2 against 0.58 mA/cm^2 . The latter remarks why a MET cathode, or electrode in general, contributes to increment losses while and EFC is working. This additional loss it is due to a lowered total reaction potential since the mediator links its reaction to the enzymatic response.

Figure 33 provides an idea on how DET is carried out: from the magnified portion of the SEM micrography various agglomerates are visible, underlining the binding effect of the TBAB modified Nafion and the presence of numerous groups of anthracene modified MWCNTs. Also,

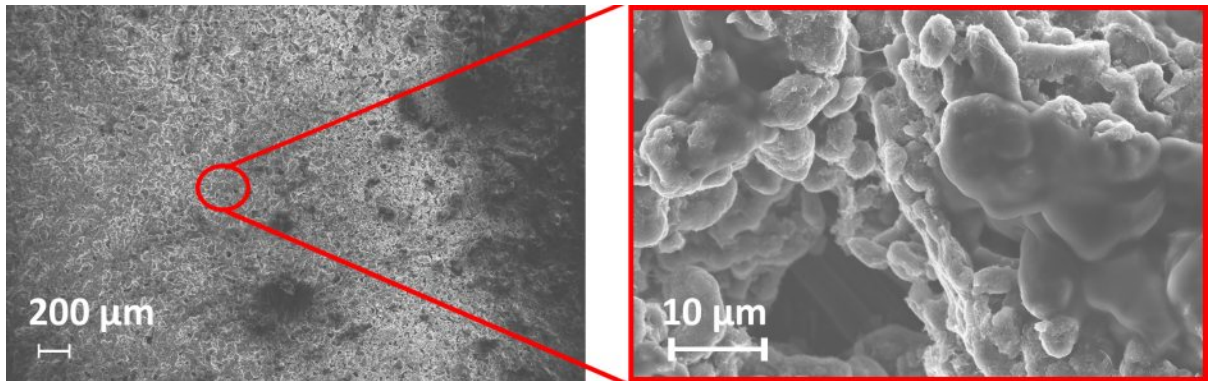


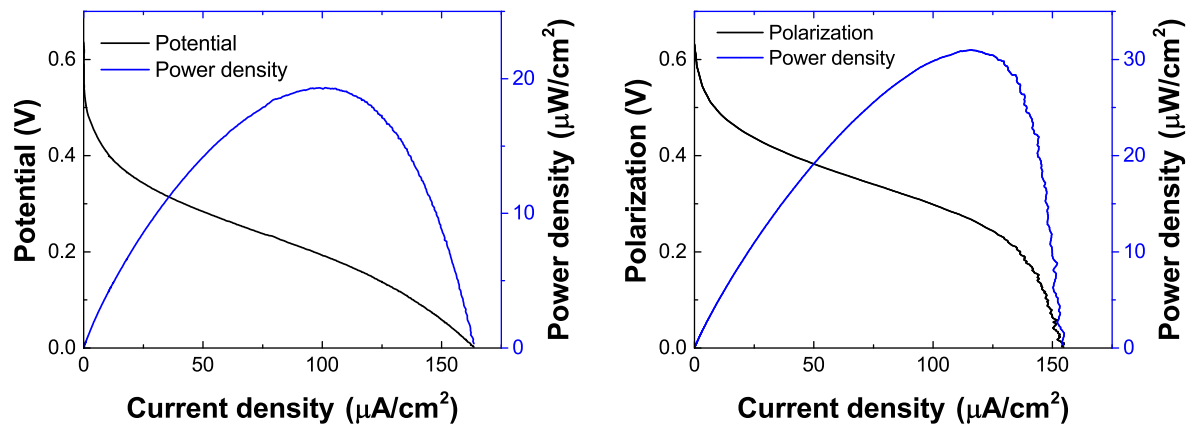
Figure 33: SEM micrograph and details of a DET toray based cathode, coated with laccase, Ac-MWCNTs and TBAB modified Nafion as a binder.

this figure shows how the employed immobilization technique results in a random orientation of the enzymes, which may be unfavorably affecting a DET.

3.3 Polarization and Power Curves

Recalling the theory explained in 1.8.5, polarization and power curves have been obtained. In particular, the upcoming figure aims to provide a useful parameter about the order of magnitude of the properties that should be expected from this kind of EFC. Both fuel cells in Fig. 34(a) and Fig. 34(b) have been coated with hexylferrocenyl-LPEI synthesized as in Ref. [71]. As expected, the laccase based cell performed better, reaching a maximum power density of $31 \mu W/cm^2$ and a short circuit current of $157 \mu A/cm^2$ against $19.4 \mu W/cm^2$ and $163.5 \mu A/cm^2$ of the bilirubin oxidase cell. Although the two cells presented a similar range of current density, the one in 34(b) reached higher power densities for both laccase properties and inferior ohmic losses (respectively 1721Ω and 1841Ω).

Since GOx has an optimum behavior for a pH between 6 and 8, BOD was selected as a MCO



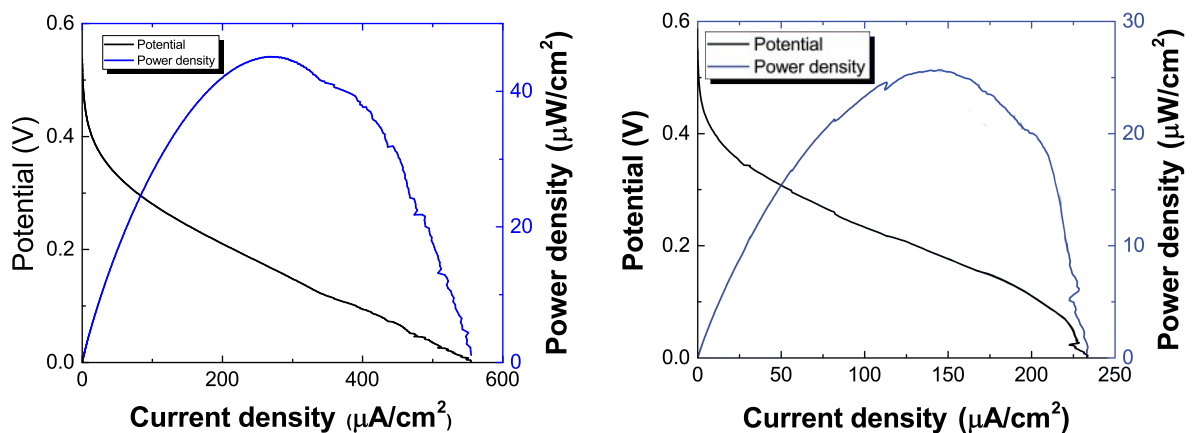
(a) Power (blue solid line) and polarization (black solid line) plots of a GOx/reference Fc- C_6 -LPEI and BOD/Ac-MWCNTs EFC. OCP and LSV were performed at pH 6.5.

(b) Power (blue solid line) and polarization (black solid line) plots of a GOx/reference Fc- C_6 -LPEI and laccase/Ac-MWCNTs EFC. OCP and LSV were performed at pH 5.

Figure 34: Power (blue solid line) and polarization (black solid line) curves comparison between a BOD and laccase based EFC, within different pH values selected within the range of optimum pH for each enzyme. OCP tests were performed prior to LSVs, which were carried out at a scan rate of 1 mV/s. The used solution contained 0.1 M of glucose and was oxygen saturated at a temperature of 26 °C.

enzyme for the cathodic coating. Thus, before building a microfluidic device, it was necessary to analyze the theoretical performances of a bilirubin oxidase and glucose oxidase fuel cell with polarization and power curves, using the self produced hexylferrocenyl-LPEI for what concerns the anodic coating. Figure 35(a) provides an immediate insight: the short circuit current is 239% higher than the one obtained in 34(a), reaching a value of 554.9 $\mu\text{A}/\text{cm}^2$. In addition

the maximum power was $45.2 \mu\text{W}/\text{cm}^2$, thus there is an increase of 133%. Furthermore, the accounted ohmic losses are 636Ω : about three times less, despite an equal setup during LSV tests (the distance between anode and cathode was kept constant at about 1.5 cm). Finally,



(a) Power (blue solid line) and polarization (black solid line) plots of a GOx/self-produced Fc- C_6 -LPEI and BOd/Ac-MWCNTs EFC. OCP and LSV were performed at pH 6.5.

(b) Power (blue solid line) and polarization (black solid line) plots of GOx/self-produced Fc- C_6 -LPEI and BOd/Ac-MWCNTs 3D printic microfluidic EFC. OCP and LSV were performed at pH 6.5. Flow was single injected with a syringe pump. The used flow rate of 0.1 mL/min.

Figure 35: Comparison of BOD and laccase based cathodes, within different pH values selected within the range of optimum pH for each enzyme. All CVs were carried using a 0.2 M citrate/phosphate buffer solution oxygen saturated, at a scan rate of 1 mV/s and temperature of 26 °C.

Figure 35(b) provides the characteristic power and polarization curves about the 3D printed microfluidic enzymatic fuel cell. LSV was performed providing a single flow of 0.1 mL/min of fuel (0.2 M citrate/phosphate buffer solution at pH 6.5) saturated with oxygen. In this latter

case, results are worst than the ones achieved during the tests of the sample electrodes ($234 \mu A/cm^2$ and $26.4 \mu W/cm^2$); on the other hand, however, they are still higher than the ones in Fig. 34(a). This steep performance decrease is mainly due to the cathodic coating: during the previous tests it has been observed a lack of ‘repeatability’ of the results which can be attributed to how the cathodic coating has been made. Coating with a brush is unavoidably less precise than using a pipette - in which volume can be controlled -, thus errors can only be multiplied when the to-be-coated surface is bigger than $1 cm^2$. In the used microfluidic design, the total area of each electrode is $6 cm^2$. Moreover, the cell was assembled with bolted joints: this leads to a compression of the layers, which ineluctably ruin the cathodic coating. The anode does not suffer from the same issue because its cloth is not made of powder material like the Ac-MWCNTs.

3.4 Life and Stability

Stability of the microfluidic EFC was evaluated: as soon as the cell was assembled, tests have been carried out by sampling with a Keithley 2701 the potential across a $22 k\Omega$ resistor. The first objective was to find the point in which the microfluidic EFC could deliver its maximum output: thus, the performed test was to observe the flow rate effects on the output voltage. To achieve an accurate and stable measure, this test was performed after 6 hours from the start up time of the microfluidic EFC. By varying flow rate values with a syringe pump model Nexus 3000, the detected voltage reaches a maximum with a flow rate of $0.1 mL/min$. From a nil fuel supply up to the $0.1 mL/min$, the output rises due to the increasing quantity of both glucose and oxygen provided to anode and cathode. After that point, voltage decreases for several

reasons: too much oxygen can disable the glucose oxidase activities, especially when the rate of oxygen supply is over the enzymatic turnover rate. The change in the measured output is immediately observed as the flow rate changes; however, all points were plotted after a wait of about twenty minutes per each flow rate value.

The second aim was to characterize the lifetime of the EFC in order to observe its lifespan and

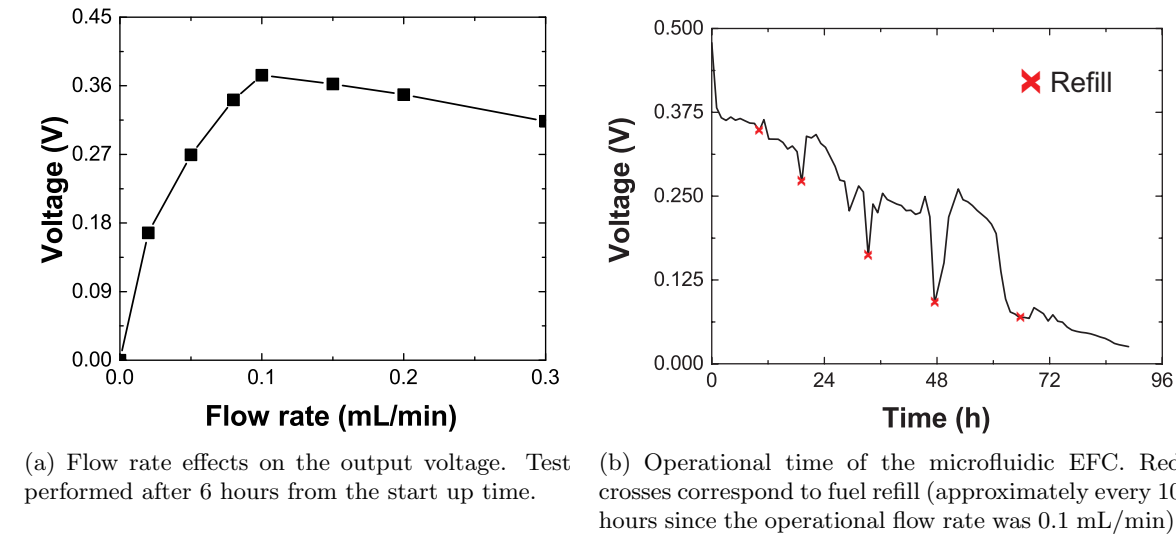


Figure 36: Relationship between flow rate and the EFC performances and monitored working time and output of the microfluidic EFC. All measurements have been carried out with a DMM model Keithley 2701 measuring the voltage across a resistor of 22 k Ω .

try to detect its actual limits. After an initial time of 24 hours in which two fuel refills were necessary, the measured voltage dropped of about 8.3% (Fig. 36(b)). Stability is among the

major advantages of an EFC, and as pointed out by Fig. 36(b), this microfluidic devices fully achieved it. This EFC's grand swan-song occurs around after 60 hours of operations: a steep drop off in the detected voltage is clear, since the potential decreases of an important 68%. On one hand this is due to the stability of the film coating the anode: from previous publications, the reference polymer had a working life of about 40 hours, but the employed and heavier hexylferrocenyl-LPEI resisted longer to degradation. On the other hand, voltage dropped also due to the peroxide production from the intermediate reduction of oxygen to water catalytically enhanced by bilirubin oxidase. It is the cathode that suffers more from H_2O_2 production: bilirubin oxidase shows a to be affected by its presence, even with removal occurring (H_2O_2 was being constantly removed by the out going flow). After that, the microfluidic device tries to provide power hand-to-mouth, with inadequate output voltage values.

CHAPTER 4

CONCLUSION

The aim and particular objectives of this thesis were presented in chapter 1 as well as background and basic principles of a microfluidic fuel cell. Particular attention was given to the electrochemical part: again, in chapter 1 several electrochemical concepts were explained as they represented a huge and fundamental part of this work. The used equipment and the steps followed for this study were described in chapter 2, whereas the consequent results have been introduced, analyzed and discussed in chapter 3. In this last chapter, conclusions are given as well as possible future development and opportunities.

For the sake of understanding and characterizing the performances, limits and challenges of an enzymatic fuel cell, the main approach was to divide the work in two parts: a purely electrochemical one and a microfluidic EFC design. The first stage aimed at observing the effects of enzyme immobilization, of the employed fuel/oxidant and the influence of its pH on the electrodes, as well as considering different materials or various coatings and explain the changes in the related properties; the last step was necessary for demonstrating the easiness and feasibility of a microfluidic system fabricated with novel advanced manufacturing techniques as a 3D-printing. Moreover, this latter was necessary to further study the enzyme stability, durability and the effect of fuel transport on the obtained electric power.

As resulting from the electrochemical tests, both anodic and cathodic coatings behaved correspondingly to the various reference papers used as inspiration for this work. Although

on one hand the achieved performances for the cathode were satisfying but not incredibly better than the published ones, the same can not be said for the anode. The hypothesis to use a longer LPEI for the production of hexylferrocenyl-LPEI in order to yield higher anodic current densities was correct. As already presented before, the reason of employing a higher molecular weight was to exploit more redox sites available to the ferrocene and therefore to the GOx enzyme. Independently from the used substrate (both toray paper and buckypaper were tested), the coating hydrogel yielded current densities at least three times higher than the hexylferrocenyl-LPEI from Ref. [71]. These advantages were still present after a reduction of 20% of both polymer and GOx ratio in the coating, resulting in a current density still double than Ref. [72]. Moreover, this self produced redox polymer has the further advantages to eliminate preparatory steps needed for the LPEI synthesis, which is not an expensive product and it comes available with different molecular weight options.

Moreover, the tested microfluidic EFC presented very good results in terms of current and power densities, coherent with the ones already reported for similar microfluidic EFCs employing the same enzymes [57; 96; 97]. The hypothesis behind the chosen design was that providing both fuel and oxidant in the same fluid flow would prolong the enzymes lifetime because the electrodes will be constantly flooded. As a consequence of the single inlet and outlet choice, since glucose oxidase has an optimum behavior for a pH between 6 and 8, bilirubin oxidase was selected as a MCO enzyme for the cathodic coating for the microfluidic design. In addition, willing and oriented to exploit affirmed trends in the advancing manufacturing techniques, the microfluidic device was produced with a stereolithography based 3D printer. In particular, the

employed material is a clear resin, able to be cured with a final resolution of 25 μm per layer, with a good bio-compatibility. Despite an air breathing cathode would have lead to better performances (in a liquid there is a lower threshold of oxygen solubility), both electrodes were designed to be flooded since this would help to miniaturize this EFC design for a stacked configuration. Following the path chosen with this thesis, further developments and ideas might include analyzing a stack of microfluidic EFC. An interesting option would be using enzyme purification techniques, changing coating, or employ an enzymatic cascade in order to enhance the cathodic performances. Further efforts EFC field must also accomplish a better understanding and development of biocatalysis, enzyme lifetimes etc. to expand the strict and narrow range of applications that can be made today.

APPENDICES

Appendix A

PERMISSIONS

Appendix A (continued)

4/9/2016

RightsLink Printable License

NATURE PUBLISHING GROUP LICENSE TERMS AND CONDITIONS

Apr 10, 2016

This is a License Agreement between Roberto Preite ("You") and Nature Publishing Group ("Nature Publishing Group") provided by Copyright Clearance Center ("CCC"). The license consists of your order details, the terms and conditions provided by Nature Publishing Group, and the payment terms and conditions.

All payments must be made in full to CCC. For payment instructions, please see information listed at the bottom of this form.

License Number	3845140453064
License date	Apr 10, 2016
Licensed content publisher	Nature Publishing Group
Licensed content publication	Nature
Licensed content title	Materials for fuel-cell technologies
Licensed content author	Brian C. H. Steele and Angelika Heinzl
Licensed content date	Nov 15, 2001
Volume number	414
Issue number	6861
Type of Use	reuse in a dissertation / thesis
Requestor type	academic/educational
Format	print and electronic
Portion	figures/tables/illustrations
Number of figures/tables/illustrations	1
Figures	# 1
Author of this NPG article	no
Your reference number	None
Title of your thesis / dissertation	DESIGN AND PERFORMANCE CHARACTERISTICS OF A MICROFLUIDIC ENZYMATIC FUEL CELL
Expected completion date	May 2016
Estimated size (number of pages)	100
Total	0.00 USD
Terms and Conditions	

Terms and Conditions for Permissions

Nature Publishing Group hereby grants you a non-exclusive license to reproduce this material for this purpose, and for no other use, subject to the conditions below:

1. NPG warrants that it has, to the best of its knowledge, the rights to license reuse of this material. However, you should ensure that the material you are requesting is original to Nature Publishing Group and does not carry the copyright of another entity (as credited in the published version). If the credit line on any part of the material you have requested indicates that it was reprinted or adapted by NPG with permission from another source, then you should also seek permission from that source to reuse the material.

Figure 37: Permission for Figure 2.

Appendix A (continued)

4/16/2016

RightsLink Printable License

**ELSEVIER LICENSE
TERMS AND CONDITIONS**

Apr 16, 2016

This is a License Agreement between Roberto Preite ("You") and Elsevier ("Elsevier") provided by Copyright Clearance Center ("CCC"). The license consists of your order details, the terms and conditions provided by Elsevier, and the payment terms and conditions.

All payments must be made in full to CCC. For payment instructions, please see information listed at the bottom of this form.

Supplier	Elsevier Limited The Boulevard, Langford Lane Kidlington, Oxford, OX5 1GB, UK
Registered Company Number	1982084
Customer name	Roberto Preite
Customer address	410 S morgan st CHICAGO, IL 60607
License number	3851001385470
License date	Apr 16, 2016
Licensed content publisher	Elsevier
Licensed content publication	Journal of Power Sources
Licensed content title	PEM fuel cell electrodes
Licensed content author	S. Litster, G. McLean
Licensed content date	3 May 2004
Licensed content volume number	130
Licensed content issue number	1-2
Number of pages	16
Start Page	61
End Page	76
Type of Use	reuse in a thesis/dissertation
Portion	figures/tables/illustrations
Number of figures/tables/illustrations	1
Format	both print and electronic
Are you the author of this Elsevier article?	No
Will you be translating?	No
Original figure numbers	fig 1
Title of your thesis/dissertation	DESIGN AND PERFORMANCE CHARACTERISTICS OF A MICROFLUIDIC ENZYMATIC FUEL CELL
Expected completion date	May 2016

<https://s100.copyright.com/AppDispatchServlet>

1/6

Figure 38: Permission for Figure 3.

Appendix A (continued)

4/9/2016

RightsLink Printable License

**ELSEVIER LICENSE
TERMS AND CONDITIONS**

Apr 10, 2016

This is a License Agreement between Roberto Preite ("You") and Elsevier ("Elsevier") provided by Copyright Clearance Center ("CCC"). The license consists of your order details, the terms and conditions provided by Elsevier, and the payment terms and conditions.

All payments must be made in full to CCC. For payment instructions, please see information listed at the bottom of this form.

Supplier	Elsevier Limited The Boulevard, Langford Lane Kidlington, Oxford, OX5 1GB, UK
Registered Company Number	1982084
Customer name	Roberto Preite
Customer address	410 S morgan st CHICAGO, IL 60607
License number	3845150373923
License date	Apr 10, 2016
Licensed content publisher	Elsevier
Licensed content publication	Journal of Power Sources
Licensed content title	Recent advances in high temperature electrolysis using solid oxide fuel cells: A review
Licensed content author	M.A. Laguna-Bercero
Licensed content date	1 April 2012
Licensed content volume number	203
Licensed content issue number	n/a
Number of pages	13
Start Page	4
End Page	16
Type of Use	reuse in a thesis/dissertation
Intended publisher of new work	other
Portion	figures/tables/illustrations
Number of figures/tables/illustrations	1
Format	both print and electronic
Are you the author of this Elsevier article?	No
Will you be translating?	No
Original figure numbers	fig 1
Title of your thesis/dissertation	DESIGN AND PERFORMANCE CHARACTERISTICS OF A MICROFLUIDIC ENZYMATIC FUEL CELL

<https://s100.copyright.com/AppDispatchServlet>

1/6

Figure 39: Permission for Figure 4.

Appendix A (continued)

4/9/2016

RightsLink Printable License

**ELSEVIER LICENSE
TERMS AND CONDITIONS**

Apr 10, 2016

This is a License Agreement between Roberto Preite ("You") and Elsevier ("Elsevier") provided by Copyright Clearance Center ("CCC"). The license consists of your order details, the terms and conditions provided by Elsevier, and the payment terms and conditions.

All payments must be made in full to CCC. For payment instructions, please see information listed at the bottom of this form.

Supplier	Elsevier Limited The Boulevard, Langford Lane Kidlington, Oxford, OX5 1GB, UK
Registered Company Number	1982084
Customer name	Roberto Preite
Customer address	410 S morgan st CHICAGO, IL 60607
License number	3845150766581
License date	Apr 10, 2016
Licensed content publisher	Elsevier
Licensed content publication	Current Opinion in Solid State & Materials Science
Licensed content title	Molten carbonate fuel cells
Licensed content author	Andrew L. Dicks
Licensed content date	October 2004
Licensed content volume number	8
Licensed content issue number	5
Number of pages	5
Start Page	379
End Page	383
Type of Use	reuse in a thesis/dissertation
Intended publisher of new work	other
Portion	figures/tables/illustrations
Number of figures/tables/illustrations	1
Format	both print and electronic
Are you the author of this Elsevier article?	No
Will you be translating?	No
Original figure numbers	fig 1
Title of your thesis/dissertation	DESIGN AND PERFORMANCE CHARACTERISTICS OF A MICROFLUIDIC ENZYMATIC FUEL CELL

<https://s100.copyright.com/AppDispatchServlet>

1/6

Figure 40: Permission for Figure 5.

Appendix A (continued)

4/10/2016

RightsLink Printable License

JOHN WILEY AND SONS LICENSE TERMS AND CONDITIONS

Apr 10, 2016

This Agreement between Roberto Preite ("You") and John Wiley and Sons ("John Wiley and Sons") consists of your license details and the terms and conditions provided by John Wiley and Sons and Copyright Clearance Center.

License Number	3845490842539
License date	Apr 10, 2016
Licensed Content Publisher	John Wiley and Sons
Licensed Content Publication	Wiley Books
Licensed Content Title	Fuel Cell Systems Explained, 2nd Edition
Licensed Content Author	James Larminie, Andrew Dicks
Licensed Content Date	Mar 1, 2003
Pages	428
Type of use	Dissertation/Thesis
Requestor type	University/Academic
Format	Print and electronic
Portion	Figure/table
Number of figures/tables	1
Original Wiley figure/table number(s)	fig 1.4
Will you be translating?	No
Title of your thesis / dissertation	DESIGN AND PERFORMANCE CHARACTERISTICS OF A MICROFLUIDIC ENZYMATIC FUEL CELL
Expected completion date	May 2016
Expected size (number of pages)	100
Requestor Location	Roberto Preite 410 S morgan st Unit 513 CHICAGO, IL 60607 United States Attn: Roberto Preite
Billing Type	Invoice
Billing Address	Roberto Preite 410 S morgan st Unit 513 CHICAGO, IL 60607 United States Attn: Roberto Preite
Total	0.00 USD
Terms and Conditions	

Figure 41: Permission for Figure 6

Appendix A (continued)

4/10/2016

RightsLink Printable License

**ELSEVIER LICENSE
TERMS AND CONDITIONS**

Apr 10, 2016

This is a License Agreement between Roberto Preite ("You") and Elsevier ("Elsevier") provided by Copyright Clearance Center ("CCC"). The license consists of your order details, the terms and conditions provided by Elsevier, and the payment terms and conditions.

All payments must be made in full to CCC. For payment instructions, please see information listed at the bottom of this form.

Supplier	Elsevier Limited The Boulevard, Langford Lane Kidlington, Oxford, OX5 1GB, UK
Registered Company Number	1982084
Customer name	Roberto Preite
Customer address	410 S morgan st CHICAGO, IL 60607
License number	3845551006026
License date	Apr 10, 2016
Licensed content publisher	Elsevier
Licensed content publication	Electrochimica Acta
Licensed content title	Enzymatic fuel cells: Recent progress
Licensed content author	Dónal Leech, Paul Kavanagh, Wolfgang Schuhmann
Licensed content date	1 December 2012
Licensed content volume number	84
Licensed content issue number	n/a
Number of pages	12
Start Page	223
End Page	234
Type of Use	reuse in a thesis/dissertation
Intended publisher of new work	other
Portion	figures/tables/illustrations
Number of figures/tables/illustrations	1
Format	both print and electronic
Are you the author of this Elsevier article?	No
Will you be translating?	No
Original figure numbers	fig 2
Title of your thesis/dissertation	DESIGN AND PERFORMANCE CHARACTERISTICS OF A MICROFLUIDIC ENZYMATIC FUEL CELL

<https://s100.copyright.com/AppDispatchServlet>

1/6

Figure 42: Permission for Figure 8.

Appendix A (continued)

4/7/2016

RightsLink Printable License

**ELSEVIER LICENSE
TERMS AND CONDITIONS**

Apr 07, 2016

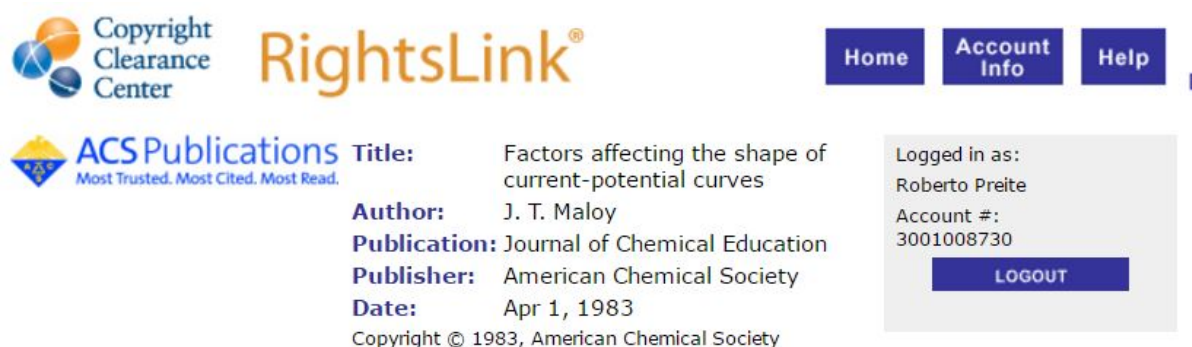
This is a License Agreement between Roberto Preite ("You") and Elsevier ("Elsevier") provided by Copyright Clearance Center ("CCC"). The license consists of your order details, the terms and conditions provided by Elsevier, and the payment terms and conditions.

All payments must be made in full to CCC. For payment instructions, please see information listed at the bottom of this form.

Supplier	Elsevier Limited The Boulevard, Langford Lane Kidlington, Oxford, OX5 1GB, UK
Registered Company Number	1982084
Customer name	Roberto Preite
Customer address	410 S morgan st CHICAGO, IL 60607
License number	3843720821150
License date	Apr 07, 2016
Licensed content publisher	Elsevier
Licensed content publication	Electrochimica Acta
Licensed content title	Direct electron transfer based enzymatic fuel cells
Licensed content author	Magnus Falk, Zoltan Blum, Sergey Shleev
Licensed content date	1 November 2012
Licensed content volume number	82
Licensed content issue number	n/a
Number of pages	12
Start Page	191
End Page	202
Type of Use	reuse in a thesis/dissertation
Portion	figures/tables/illustrations
Number of figures/tables/illustrations	2
Format	both print and electronic
Are you the author of this Elsevier article?	No
Will you be translating?	No
Original figure numbers	table 1
Title of your thesis/dissertation	DESIGN AND PERFORMANCE CHARACTERISTICS OF A MICROFLUIDIC ENZYMATIC FUEL CELL
Expected completion date	May 2016

Figure 43: Permission for Table VII.

Appendix A (continued)



The screenshot shows the Copyright Clearance Center RightsLink interface. At the top, there are logos for the Copyright Clearance Center and ACS Publications, along with navigation buttons for Home, Account Info, and Help. The main content area displays the details of a requested permission for a publication titled "Factors affecting the shape of current-potential curves" by J. T. Maloy, published in the Journal of Chemical Education by the American Chemical Society in April 1983. A sidebar on the right shows the user is logged in as Roberto Preite with account number 3001008730 and a Logout button. The bottom section contains a statement that permission is granted at no charge, followed by a list of conditions and a note about obtaining credit from other sources.

Copyright Clearance Center **RightsLink®** [Home](#) [Account Info](#) [Help](#) [L](#)

ACS Publications Most Trusted. Most Cited. Most Read.

Title: Factors affecting the shape of current-potential curves
Author: J. T. Maloy
Publication: Journal of Chemical Education
Publisher: American Chemical Society
Date: Apr 1, 1983
 Copyright © 1983, American Chemical Society

Logged in as:
 Roberto Preite
 Account #:
 3001008730
[LOGOUT](#)

PERMISSION/LICENSE IS GRANTED FOR YOUR ORDER AT NO CHARGE

This type of permission/license, instead of the standard Terms & Conditions, is sent to you because no fee is being charged for your order. Please note the following:




- Permission is granted for your request in both print and electronic formats, and translations.
- If figures and/or tables were requested, they may be adapted or used in part.
- Please print this page for your records and send a copy of it to your publisher/graduate school.
- Appropriate credit for the requested material should be given as follows: "Reprinted (adapted) with permission from (COMPLETE REFERENCE CITATION). Copyright (YEAR) American Chemical Society." Insert appropriate information in place of the capitalized words.
- One-time permission is granted only for the use specified in your request. No additional uses are granted (such as derivative works or other editions). For any other uses, please submit a new request.


If credit is given to another source for the material you requested, permission must be obtained from that source.

Figure 44: Permission for Figure 9, Figure 12 and Figure 13.

Appendix A (continued)

4/10/2016 Rightslink® by Copyright Clearance Center



[Home](#) [Account Info](#) [Help](#)  Live Chat


Title: Electrochemistry of Fullerenes and Their Derivatives
Author: Luis Echegoyen, Lourdes E. Echegoyen
Publication: Accounts of Chemical Research
Publisher: American Chemical Society
Date: Sep 1, 1998
 Copyright © 1998, American Chemical Society

Logged in as: Roberto Preite
 Account #: 3001008730
[LOGOUT](#)

PERMISSION/LICENSE IS GRANTED FOR YOUR ORDER AT NO CHARGE

This type of permission/license, instead of the standard Terms & Conditions, is sent to you because no fee is being charged for your order. Please note the following:

- Permission is granted for your request in both print and electronic formats, and translations.
- If figures and/or tables were requested, they may be adapted or used in part.
- Please print this page for your records and send a copy of it to your publisher/graduate school.
- Appropriate credit for the requested material should be given as follows: "Reprinted (adapted) with permission from (COMPLETE REFERENCE CITATION). Copyright (YEAR) American Chemical Society." Insert appropriate information in place of the capitalized words.
- One-time permission is granted only for the use specified in your request. No additional uses are granted (such as derivative works or other editions). For any other uses, please submit a new request.

If credit is given to another source for the material you requested, permission must be obtained from that source.

[BACK](#)[CLOSE WINDOW](#)

Copyright © 2016 Copyright Clearance Center, Inc. All Rights Reserved. [Privacy statement](#). [Terms and Conditions](#).
 Comments? We would like to hear from you. E-mail us at customercare@copyright.com

Figure 45: Permission for Figure 11.

Appendix A (continued)

3/29/2016 Rightslink® by Copyright Clearance Center

Copyright Clearance Center **RightsLink®** Home Create Account Help Live Chat

ACS Publications **Title:** Effect of Mediator Spacing on Electrochemical and Enzymatic Response of Ferrocene Redox Polymers

Author: Stephen A. Merchant, Matthew T. Meredith, Tu O. Tran, et al

Publication: The Journal of Physical Chemistry C

Publisher: American Chemical Society

Date: Jul 1, 2010

Copyright © 2010, American Chemical Society

LOGIN
If you're a copyright.com user, you can login to RightsLink using your copyright.com credentials. Already a RightsLink user or want to learn more?

PERMISSION/LICENSE IS GRANTED FOR YOUR ORDER AT NO CHARGE

This type of permission/license, instead of the standard Terms & Conditions, is sent to you because no fee is being charged for your order. Please note the following:

- Permission is granted for your request in both print and electronic formats, and translations.
- If figures and/or tables were requested, they may be adapted or used in part.
- Please print this page for your records and send a copy of it to your publisher/graduate school.
- Appropriate credit for the requested material should be given as follows: "Reprinted (adapted) with permission from (COMPLETE REFERENCE CITATION). Copyright (YEAR) American Chemical Society." Insert appropriate information in place of the capitalized words.
- One-time permission is granted only for the use specified in your request. No additional uses are granted (such as derivative works or other editions). For any other uses, please submit a new request.

If credit is given to another source for the material you requested, permission must be obtained from that source.


BACK

CLOSE WINDOW

Copyright © 2016 Copyright Clearance Center, Inc. All Rights Reserved. [Privacy statement](#). [Terms and Conditions](#). Comments? We would like to hear from you. E-mail us at customer@copyright.com

Figure 46: Permission for Figure 17 and Figure 18.

Appendix A (continued)




[Home](#)
[Account Info](#)
[Help](#)



Title: Crystal Structure of a Four-Copper Laccase Complexed with an Arylamine: Insights into Substrate Recognition and Correlation with Kinetics,

Author: Thomas Bertrand, Claude Jolival, Pierre Briozzo, et al

Publication: Biochemistry

Publisher: American Chemical Society

Date: Jun 1, 2002

Copyright © 2002, American Chemical Society

Logged in as:
Roberto Preite
Account #:
3001008730

[LOGOUT](#)

PERMISSION/LICENSE IS GRANTED FOR YOUR ORDER AT NO CHARGE

This type of permission/license, instead of the standard Terms & Conditions, is sent to you because no fee is being charged for your order. Please note the following:

- Permission is granted for your request in both print and electronic formats, and translations.
- If figures and/or tables were requested, they may be adapted or used in part.
- Please print this page for your records and send a copy of it to your publisher/graduate school.
- Appropriate credit for the requested material should be given as follows: "Reprinted (adapted) with permission from (COMPLETE REFERENCE CITATION). Copyright (YEAR) American Chemical Society." Insert appropriate information in place of the capitalized words.
- One-time permission is granted only for the use specified in your request. No additional uses are granted (such as derivative works or other editions). For any other uses, please submit a new request.

If credit is given to another source for the material you requested, permission must be obtained from that source.

Figure 47: Permission for Figure 22.

Appendix A (continued)

4/6/2016

RightsLink Printable License

**ROYAL SOCIETY OF CHEMISTRY LICENSE
TERMS AND CONDITIONS**

Apr 06, 2016

This Agreement between Roberto Preite ("You") and Royal Society of Chemistry ("Royal Society of Chemistry") consists of your license details and the terms and conditions provided by Royal Society of Chemistry and Copyright Clearance Center.

License Number	3843281164363
License date	Apr 06, 2016
Licensed Content Publisher	Royal Society of Chemistry
Licensed Content Publication	Chemical Communications (Cambridge)
Licensed Content Title	Bilirubin oxidase bioelectrocatalytic cathodes: the impact of hydrogen peroxide
Licensed Content Author	Ross D. Milton,Fabien Giroud,Alfred E. Thumser,Shelley D. Minter,Robert C. T. Slade
Licensed Content Date	Oct 29, 2013
Licensed Content Volume Number	50
Licensed Content Issue Number	1
Type of Use	Thesis/Dissertation
Requestor type	academic/educational
Portion	figures/tables/images
Number of figures/tables/images	1
Format	print and electronic
Distribution quantity	1000
Will you be translating?	no
Order reference number	None
Title of the thesis/dissertation	DESIGN AND PERFORMANCE CHARACTERISTICS OF A MICROFLUIDIC ENZYMATIC FUEL CELL
Expected completion date	May 2016
Estimated size	100
Requestor Location	Roberto Preite 410 S morgan st Unit 513 CHICAGO, IL 60607 United States Attn: Roberto Preite
Billing Type	Invoice
Billing Address	Roberto Preite 410 S morgan st Unit 513 CHICAGO, IL 60607

Figure 48: Permission for Figure 26.

Appendix A (continued)

4/15/2016

RightsLink Printable License

SPRINGER LICENSE TERMS AND CONDITIONS

Apr 15, 2016

This is a License Agreement between Roberto Preite ("You") and Springer ("Springer") provided by Copyright Clearance Center ("CCC"). The license consists of your order details, the terms and conditions provided by Springer, and the payment terms and conditions.

All payments must be made in full to CCC. For payment instructions, please see information listed at the bottom of this form.

License Number	3850330529954
License date	Apr 15, 2016
Licensed content publisher	Springer
Licensed content publication	Microfluids and Nanofluids
Licensed content title	3D printing: an emerging tool for novel microfluidics and lab-on-a-chip applications
Licensed content author	Alireza Ahmadian Yazdi
Licensed content date	Jan 1, 2016
Volume number	20
Issue number	3
Type of Use	Thesis/Dissertation
Portion	Figures/tables/illustrations
Number of figures/tables/illustrations	1
Author of this Springer article	No
Order reference number	None
Original figure numbers	fig 1
Title of your thesis / dissertation	DESIGN AND PERFORMANCE CHARACTERISTICS OF A MICROFLUIDIC ENZYMATIC FUEL CELL
Expected completion date	May 2016
Estimated size(pages)	100
Total	0.00 USD
Terms and Conditions	

Introduction

The publisher for this copyrighted material is Springer. By clicking "accept" in connection with completing this licensing transaction, you agree that the following terms and conditions apply to this transaction (along with the Billing and Payment terms and conditions established by Copyright Clearance Center, Inc. ("CCC"), at the time that you opened your Rightslink account and that are available at any time at <http://myaccount.copyright.com>).

Limited License

With reference to your request to reuse material on which Springer controls the copyright, permission is granted for the use indicated in your enquiry under the following conditions:
 - Licenses are for one-time use only with a maximum distribution equal to the number stated in your request.

Figure 49: Permission for Figure 27(a).

CITED LITERATURE

1. BP: Statistical review of world energy 2014, workbook (xlsx). Workbook (Xlsx), 2014.
2. Nakicenovic, N. and Swart, R.: Special report on emissions scenarios. Special Report on Emissions Scenarios, Edited by Nebojsa Nakicenovic and Robert Swart, pp. 612. ISBN 0521804930. Cambridge, UK: Cambridge University Press, July 2000., 1, 2000.
3. Berndes, G., Hoogwijk, M., and van den Broek, R.: The contribution of biomass in the future global energy supply: a review of 17 studies. Biomass and bioenergy, 25(1):1–28, 2003.
4. Yamamoto, H., Yamaji, K., and Fujino, J.: Evaluation of bioenergy resources with a global land use and energy model formulated with sd technique. Applied Energy, 63(2):101–113, 1999.
5. Dyer, C. K.: Fuel cells for portable applications. Journal of Power Sources, 106(1):31–34, 2002.
6. O’Hayre, R. P., Cha, S.-W., Colella, W., and Prinz, F. B.: Fuel cell fundamentals. John Wiley & Sons New York, 2006.
7. Steele, B. C. and Heinzel, A.: Materials for fuel-cell technologies. Nature, 414(6861):345–352, 2001.
8. Litster, S. and McLean, G.: Pem fuel cell electrodes. Journal of Power Sources, 130(1):61–76, 2004.
9. Sopian, K. and Daud, W. R. W.: Challenges and future developments in proton exchange membrane fuel cells. Renewable Energy, 31(5):719–727, 2006.
10. Amphlett, J., Baumert, R., Mann, R., Peppley, B., Roberge, R., and Rodrigues, A.: The effect of carbon monoxide contamination on anode efficiency in pem fuel cells. PREPRINTS OF PAPERS-AMERICAN CHEMICAL SOCIETY DIVISION FUEL CHEMISTRY, 38:1477–1477, 1993.

CITED LITERATURE (continued)

11. Mehta, V. and Cooper, J. S.: Review and analysis of pem fuel cell design and manufacturing. Journal of Power Sources, 114(1):32–53, 2003.
12. Lin, G. and Van Nguyen, T.: Effect of thickness and hydrophobic polymer content of the gas diffusion layer on electrode flooding level in a pemfc. Journal of The Electrochemical Society, 152(10):A1942–A1948, 2005.
13. Curtin, D. E., Lousenberg, R. D., Henry, T. J., Tangeman, P. C., and Tisack, M. E.: Advanced materials for improved pemfc performance and life. Journal of power Sources, 131(1):41–48, 2004.
14. Tao, S. and Irvine, J. T.: A redox-stable efficient anode for solid-oxide fuel cells. Nature materials, 2(5):320–323, 2003.
15. Shao, Z. and Haile, S. M.: A high-performance cathode for the next generation of solid-oxide fuel cells. Nature, 431(7005):170–173, 2004.
16. Laguna-Bercero, M.: Recent advances in high temperature electrolysis using solid oxide fuel cells: A review. Journal of Power Sources, 203:4–16, 2012.
17. Fabbri, E., Bi, L., Pergolesi, D., and Traversa, E.: Towards the next generation of solid oxide fuel cells operating below 600 c with chemically stable proton-conducting electrolytes. Advanced Materials, 24(2):195–208, 2012.
18. Jiang, S. P.: Nanoscale and nano-structured electrodes of solid oxide fuel cells by infiltration: advances and challenges. international journal of hydrogen energy, 37(1):449–470, 2012.
19. Massardo, A. and Lubelli, F.: Internal reforming solid oxide fuel cell-gas turbine combined cycles (irsofc-gt): Part a cell model and cycle thermodynamic analysis. In ASME 1998 International Gas Turbine and Aeroengine Congress and Exhibition, pages V003T08A028–V003T08A028. American Society of Mechanical Engineers, 1998.
20. Dicks, A. L.: Molten carbonate fuel cells. Current Opinion in Solid State and Materials Science, 8(5):379–383, 2004.
21. Kuk, S. T., Song, Y. S., and Kim, K.: Properties of a new type of cathode for molten carbonate fuel cells. Journal of power sources, 83(1):50–56, 1999.

CITED LITERATURE (continued)

22. Cherepy, N. J., Krueger, R., Fiet, K. J., Jankowski, A. F., and Cooper, J. F.: Direct conversion of carbon fuels in a molten carbonate fuel cell. Journal of the Electrochemical Society, 152(1):A80–A87, 2005.
23. Zhu, X.-J. and Huang, B.: Molten carbonate fuel cells. Electrochemical Technologies for Energy Storage and Conversion, Volume 1&2, pages 729–775, 2011.
24. Matsumoto, T., Komatsu, T., Arai, K., Yamazaki, T., Kijima, M., Shimizu, H., Takasawa, Y., and Nakamura, J.: Reduction of pt usage in fuel cell electrocatalysts with carbon nanotube electrodes. Chemical communications, (7):840–841, 2004.
25. Uchida, H., Arisaka, S., and Watanabe, M.: High performance electrodes for medium-temperature solid oxide fuel cells: Activation of la (sr) coo 3 cathode with highly dispersed pt metal electrocatalysts. Solid State Ionics, 135(1):347–351, 2000.
26. Yoshitake, T., Shimakawa, Y., Kuroshima, S., Kimura, H., Ichihashi, T., Kubo, Y., Kasuya, D., Takahashi, K., Kokai, F., Yudasaka, M., et al.: Preparation of fine platinum catalyst supported on single-wall carbon nanohorns for fuel cell application. Physica B: Condensed Matter, 323(1):124–126, 2002.
27. Larminie, J., Dicks, A., and McDonald, M. S.: Fuel cell systems explained, volume 2. Wiley New York, 2003.
28. Ivanov, I., Vidakovi-Koch, T., and Sundmacher, K.: Recent advances in enzymatic fuel cells: Experiments and modeling. Energies, 3(4):803, 2010.
29. Palmore, G. T. R. and Whitesides, G. M.: Microbial and enzymatic biofuel cells. Enzymatic conversion of biomass for fuels production, 566:271–290, 1994.
30. Kim, B. H., Chang, I. S., Gil, G. C., Park, H. S., and Kim, H. J.: Novel bod (biological oxygen demand) sensor using mediator-less microbial fuel cell. Biotechnology letters, 25(7):541–545, 2003.
31. Kim, J., Jia, H., and Wang, P.: Challenges in biocatalysis for enzyme-based biofuel cells. Biotechnology advances, 24(3):296–308, 2006.
32. He, Z., Minteer, S. D., and Angenent, L. T.: Electricity generation from artificial wastewater using an upflow microbial fuel cell. Environmental science & technology, 39(14):5262–5267, 2005.

CITED LITERATURE (continued)

33. Minteer, S. D., Liaw, B. Y., and Cooney, M. J.: Enzyme-based biofuel cells. Current opinion in biotechnology, 18(3):228–234, 2007.
34. Leech, D., Kavanagh, P., and Schuhmann, W.: Enzymatic fuel cells: Recent progress. Electrochimica Acta, 84:223–234, 2012.
35. Heller, A.: Integrated medical feedback systems for drug delivery. AIChE journal, 51(4):1054–1066, 2005.
36. Shleev, S., Tkac, J., Christenson, A., Ruzgas, T., Yaropolov, A. I., Whittaker, J. W., and Gorton, L.: Direct electron transfer between copper-containing proteins and electrodes. Biosensors and Bioelectronics, 20(12):2517–2554, 2005.
37. Falk, M., Blum, Z., and Shleev, S.: Direct electron transfer based enzymatic fuel cells. Electrochimica Acta, 82:191–202, 2012.
38. Tarasevich, M., Bogdanovskaya, V., Zagudaeva, N., and Kapustin, A.: Composite materials for direct bioelectrocatalysis of the hydrogen and oxygen reactions in biofuel cells. Russian journal of electrochemistry, 38(3):335–335, 2002.
39. Vincent, K. A., Cracknell, J. A., Lenz, O., Zebger, I., Friedrich, B., and Armstrong, F. A.: Electrocatalytic hydrogen oxidation by an enzyme at high carbon monoxide or oxygen levels. Proceedings of the National Academy of Sciences of the United States of America, 102(47):16951–16954, 2005.
40. Ramanavicius, A., Kausaite, A., and Ramanaviciene, A.: Biofuel cell based on direct bioelectrocatalysis. Biosensors and Bioelectronics, 20(10):1962–1967, 2005.
41. Kamitaka, Y., Tsujimura, S., Setoyama, N., Kajino, T., and Kano, K.: Fructose/dioxygen biofuel cell based on direct electron transfer-type bioelectrocatalysis. Physical Chemistry Chemical Physics, 9(15):1793–1801, 2007.
42. Wu, X., Zhao, F., Varcoe, J. R., Thumser, A. E., Avignone-Rossa, C., and Slade, R. C.: Direct electron transfer of glucose oxidase immobilized in an ionic liquid reconstituted cellulose–carbon nanotube matrix. Bioelectrochemistry, 77(1):64–68, 2009.
43. Coman, V., Vaz-Domínguez, C., Ludwig, R., Harreither, W., Haltrich, D., De Lacey, A. L., Ruzgas, T., Gorton, L., and Shleev, S.: A membrane-, mediator-, cofactor-less glucose/oxygen biofuel cell. Physical Chemistry Chemical Physics, 10(40):6093–6096, 2008.

CITED LITERATURE (continued)

44. Coman, V., Ludwig, R., Harreither, W., Haltrich, D., Gorton, L., Ruzgas, T., and Shleev, S.: A direct electron transfer-based glucose/oxygen biofuel cell operating in human serum. Fuel cells, 10(1):9–16, 2010.
45. Zebda, A., Gondran, C., Le Goff, A., Holzinger, M., Cinquin, P., and Cosnier, S.: Mediatorless high-power glucose biofuel cells based on compressed carbon nanotube-enzyme electrodes. Nature communications, 2:370, 2011.
46. Wang, X., Falk, M., Ortiz, R., Matsumura, H., Bobacka, J., Ludwig, R., Bergelin, M., Gorton, L., and Shleev, S.: Mediatorless sugar/oxygen enzymatic fuel cells based on gold nanoparticle-modified electrodes. Biosensors and Bioelectronics, 31(1):219–225, 2012.
47. Sarma, A. K., Vatsyayan, P., Goswami, P., and Minteer, S. D.: Recent advances in material science for developing enzyme electrodes. Biosensors and Bioelectronics, 24(8):2313–2322, 2009.
48. Rasmussen, M., Abdellaoui, S., and Minteer, S. D.: Enzymatic biofuel cells: 30 years of critical advancements. Biosensors and Bioelectronics, 76:91–102, 2016.
49. Calabrese Barton, S., Gallaway, J., and Atanassov, P.: Enzymatic biofuel cells for implantable and microscale devices. Chemical reviews, 104(10):4867–4886, 2004.
50. Reid, R. C., Minteer, S. D., and Gale, B. K.: Contact lens biofuel cell tested in a synthetic tear solution. Biosensors and Bioelectronics, 68:142–148, 2015.
51. Maloy, J.: Factors affecting the shape of current-potential curves. Journal of Chemical Education, 60(4):285, 1983.
52. Helmholtz, H.: Ueber einige gesetze der vertheilung elektrischer strme in krperlichen leitern mit anwendung auf die thierisch-elektrischen versuche. Annalen der Physik, 165(6):211–233, 1853.
53. Echegoyen, L. and Echegoyen, L. E.: Electrochemistry of fullerenes and their derivatives. Accounts of chemical research, 31(9):593–601, 1998.
54. Wang, J.: Analytical electrochemistry. John Wiley & Sons, 2006.
55. Zoski, C. G.: Handbook of Electrochemistry. Burlington, MA, Elsevier, 2007.

CITED LITERATURE (continued)

56. Bard, A. J. and Faulkner, L. R.: Electrochemical methods : fundamentals and applications. New York, Chichester, Weinheim, J. Wiley & Sons, 2001.
57. Villarrubia, C. W. N., Lau, C., Ciniciato, G. P., Garcia, S. O., Sibbett, S. S., Petsev, D. N., Babanova, S., Gupta, G., and Atanassov, P.: Practical electricity generation from a paper based biofuel cell powered by glucose in ubiquitous liquids. Electrochemistry Communications, 45:44–47, 2014.
58. Xu, S. and Minteer, S. D.: Enzymatic biofuel cell for oxidation of glucose to co₂. ACS Catalysis, 2(1):91–94, 2011.
59. Wong, C. M., Wong, K. H., and Chen, X. D.: Glucose oxidase: natural occurrence, function, properties and industrial applications. Applied microbiology and biotechnology, 78(6):927–938, 2008.
60. Muller, D.: Oxidation von glukose mit extrakten aus aspegillus niger. Biochem Z, 199:136–170, 1928.
61. Sandholm, M., Ali-Vehmas, T., Kaartinen, L., and Junnila, M.: Glucose oxidase (god) as a source of hydrogen peroxide for the lactoperoxidase (lpo) system in milk: Antibacterial effect of the god-lpo system against mastitis pathogens. Journal of Veterinary Medicine, Series B, 35(1-10):346–352, 1988.
62. Vemulapalli, V. and Hosene, R.: Glucose oxidase effects on gluten and water solubles 1. Cereal Chemistry, 75(6):859–862, 1998.
63. Figoni, P.: How Baking Works: Exploring the Fundamentals of Baking Science. Wiley, 2010.
64. Seifu, E., Buys, E. M., and Donkin, E.: Significance of the lactoperoxidase system in the dairy industry and its potential applications: a review. Trends in Food Science & Technology, 16(4):137–154, 2005.
65. Wilson, R. and Turner, A.: Glucose oxidase: an ideal enzyme. Biosensors and Bioelectronics, 7(3):165–185, 1992.
66. Book, G.: Compendium of chemical terminology. 2014.

CITED LITERATURE (continued)

67. Tsuge, H., Natsuaki, O., and Ohashi, K.: Purification, properties, and molecular features of glucose oxidase from *aspergillus niger*. Journal of Biochemistry, 78(4):835–843, 1975.
68. Swoboda, B. E. and Massey, V.: Purification and properties of the glucose oxidase from *aspergillus niger*. Journal of Biological Chemistry, 240(5):2209–2215, 1965.
69. Inzelt, G.: Mechanism of charge transport in polymer-modified electrodes. Electroanalytical chemistry, 18:89–241, 1994.
70. Gracia, R. and Mecerreyes, D.: Polymers with redox properties: materials for batteries, biosensors and more. Polymer Chemistry, 4(7):2206–2214, 2013.
71. Merchant, S. A., Meredith, M. T., Tran, T. O., Brunski, D. B., Johnson, M. B., Glatzhofer, D. T., and Schmidtke, D. W.: Effect of mediator spacing on electrochemical and enzymatic response of ferrocene redox polymers. The Journal of Physical Chemistry C, 114(26):11627–11634, 2010.
72. Merchant, S. A., Glatzhofer, D. T., and Schmidtke, D. W.: Effects of electrolyte and pH on the behavior of cross-linked films of ferrocene-modified poly (ethylenimine). Langmuir, 23(22):11295–11302, 2007.
73. Ruiz, J., Medel, M. J. R., Daniel, M.-C., Blais, J.-C., and Astruc, D.: Redox-robust pentamethylamidoferrocenyl metallodendrimers that cleanly and selectively recognize the h_2 po 4- anion. Chemical Communications, (4):464–465, 2003.
74. Reynes, O., Moutet, J.-C., Royal, G., and Saint-Aman, E.: Electrochemical sensing of anions by (ferrocenylmethyl) trialkylammonium cations in homogeneous solution and in polymer films. Electrochimica acta, 49(22):3727–3735, 2004.
75. Suzuki, M., Kobayashi, S., Kimura, M., Hanabusa, K., Shirai, H., and Kurimura, Y.: Intra-polymer electron-transfer reaction between partially quaternized poly (1-vinylimidazole) and a cobalt (ii) schiff-base complex: effect of alkyl chain length. J. Chem. Soc., Faraday Trans., 92(22):4511–4513, 1996.
76. Mao, F., Mano, N., and Heller, A.: Long tethers binding redox centers to polymer backbones enhance electron transport in enzyme wiring hydrogels. Journal of the American Chemical Society, 125(16):4951–4957, 2003.

CITED LITERATURE (continued)

77. Merchant, S. A., Tran, T. O., Meredith, M. T., Cline, T. C., Glatzhofer, D. T., and Schmidtke, D. W.: High-sensitivity amperometric biosensors based on ferrocene-modified linear poly (ethylenimine). Langmuir, 25(13):7736–7742, 2009.
78. Flory, P. J.: Principles of polymer chemistry. Cornell University Press, 1953.
79. Meredith, M. T., Kao, D.-Y., Hickey, D., Schmidtke, D. W., and Glatzhofer, D. T.: High current density ferrocene-modified linear poly (ethylenimine) bioanodes and their use in biofuel cells. Journal of the Electrochemical Society, 158(2):B166–B174, 2011.
80. Cracknell, J. A., Vincent, K. A., and Armstrong, F. A.: Enzymes as working or inspirational electrocatalysts for fuel cells and electrolysis. Chemical Reviews, 108(7):2439–2461, 2008.
81. Otsuka, K., Sugihara, T., Tsujino, Y., Osakai, T., and Tamiya, E.: Electrochemical consideration on the optimum pH of bilirubin oxidase. Analytical biochemistry, 370(1):98–106, 2007.
82. Brocato, S., Lau, C., and Atanassov, P.: Mechanistic study of direct electron transfer in bilirubin oxidase. Electrochimica Acta, 61:44–49, 2012.
83. Tsujimura, S., Kano, K., and Ikeda, T.: Bilirubin oxidase in multiple layers catalyzes four-electron reduction of dioxygen to water without redox mediators. Journal of Electroanalytical Chemistry, 576(1):113–120, 2005.
84. Bertrand, T., Jolival, C., Briozzo, P., Caminade, E., Joly, N., Madzak, C., and Mougín, C.: Crystal structure of a four-copper laccase complexed with an arylamine: insights into substrate recognition and correlation with kinetics. Biochemistry, 41(23):7325–7333, 2002.
85. Church, S.: Del. firm installs fuel cell, the news journal, p. B7, January, 6, 2006.
86. Redepenning, J. and Anson, F. C.: Permselectivities of polyelectrolyte electrode coatings as inferred from measurements with incorporated redox probes or concentration cells. The Journal of Physical Chemistry, 91(17):4549–4553, 1987.
87. Klotzbach, T., Watt, M., Ansari, Y., and Minteer, S. D.: Effects of hydrophobic modification of chitosan and nafion on transport properties, ion-exchange capacities, and enzyme immobilization. Journal of Membrane Science, 282(1):276–283, 2006.

CITED LITERATURE (continued)

88. Meredith, S., Xu, S., Meredith, M. T., and Minteer, S. D.: Hydrophobic salt-modified nafion for enzyme immobilization and stabilization. Journal of visualized experiments: JoVE, (65), 2012.
89. Akers, N. L., Moore, C. M., and Minteer, S. D.: Development of alcohol/o₂ biofuel cells using salt-extracted tetrabutylammonium bromide/nafion membranes to immobilize dehydrogenase enzymes. Electrochimica Acta, 50(12):2521–2525, 2005.
90. Thomas, T. J., Ponnusamy, K. E., Chang, N. M., Galmore, K., and Minteer, S. D.: Effects of annealing on mixture-cast membranes of nafion® and quaternary ammonium bromide salts. Journal of membrane science, 213(1):55–66, 2003.
91. Sun, Y.-P., Fu, K., Lin, Y., and Huang, W.: Functionalized carbon nanotubes: properties and applications. Accounts of Chemical Research, 35(12):1096–1104, 2002.
92. Chen, R. J., Zhang, Y., Wang, D., and Dai, H.: Noncovalent sidewall functionalization of single-walled carbon nanotubes for protein immobilization. Journal of the American Chemical Society, 123(16):3838–3839, 2001.
93. Milton, R. D., Giroud, F., Thumser, A. E., Minteer, S. D., and Slade, R. C.: Bilirubin oxidase bioelectrocatalytic cathodes: the impact of hydrogen peroxide. Chemical Communications, 50(1):94–96, 2014.
94. Minson, M., Meredith, M. T., Shrier, A., Giroud, F., Hickey, D., Glatzhofer, D. T., and Minteer, S. D.: High performance glucose/o₂ biofuel cell: Effect of utilizing purified laccase with anthracene-modified multi-walled carbon nanotubes. Journal of The Electrochemical Society, 159(12):G166–G170, 2012.
95. Yazdi, A. A., Popma, A., Wong, W., Nguyen, T., Pan, Y., and Xu, J.: 3d printing: an emerging tool for novel microfluidics and lab-on-a-chip applications. Microfluidics and Nanofluidics, 20(3):1–18, 2016.
96. González-Guerrero, M. J., Esquivel, J. P., Sánchez-Molas, D., Godignon, P., Muñoz, F. X., Del Campo, F. J., Giroud, F., Minteer, S. D., and Sabaté, N.: Membraneless glucose/o₂ microfluidic enzymatic biofuel cell using pyrolyzed photoresist film electrodes. Lab on a Chip, 13(15):2972–2979, 2013.
97. Beneyton, T., Wijaya, I. P. M., Salem, C. B., Griffiths, A., and Taly, V.: Membraneless glucose/o₂ microfluidic biofuel cells using covalently bound enzymes. Chemical Communications, 49(11):1094–1096, 2013.

VITA

NAME	Roberto Preite
<hr/>	
EDUCATION	
	Master of Science in Mechanical Engineering, University of Illinois at Chicago, August 2016, USA
	Specialization Degree in Mechanical Engineering, July 2016, Polytechnic of Turin, Italy
	Bachelor's Degree in Mechanical Engineering, July 2014, Polytechnic of Turin, Italy
<hr/>	
LANGUAGE SKILLS	
Italian	Native
English	Full working proficiency
	2013 - IELTS examination (7/9)
	A.Y. 2015/16 One Year of study abroad in Chicago, Illinois
	A.Y. 2015/16. Lessons and exams attended exclusively in English
<hr/>	
SCHOLARSHIPS	
Fall 2015	Italian scholarship for final project (thesis) at UIC
<hr/>	